Current Opinion in Colloid & Interface Science 19 (2014) 320–335

Contents lists available at ScienceDirect

Current Opinion in Colloid & Interface Science

journal homepage: www.elsevier.com/locate/cocis

Liquids on porous layers: wetting, imbibition and transport processes

Tatiana Gambaryan-Roisman

Institute of Technical Thermodynamics, Technische Universität Darmstadt, Alarich-Weiss-Str. 10, 64287 Darmstadt, Germany
Center of Smart Interfaces, Technische Universität Darmstadt, Alarich-Weiss-Str. 10, 64287 Darmstadt, Germany

ARTICLE INFO

Article history:
Received 16 January 2014
Received in revised form 1 September 2014
Accepted 2 September 2014
Available online 6 September 2014

Keywords:
Spreading
Imbibition
Porous media
Wetting transition
Nanofiber mat
Heat transfer enhancement
Cooling
Particles deposition

ABSTRACT

Wetting of porous layers plays an important role in natural phenomena and in technical applications, including cooling technologies, ink-jet printing, functionalization of textile fabric and 3D-printing. In many technically relevant processes the complex wetting phenomena govern the transport of heat, mass and (nano)particles. A review of recent advances in understanding and development of prediction tools describing the coupled wetting and transport in porous layers is given. A special focus is laid on fibrous media, which are frequently encountered as natural substances (human hair), as conventional technological products (textile fabric) or as promising method for heat transfer enhancement (nanofiber mat coating of surfaces). The possible directions of future research are suggested.

1. Introduction

Understanding the wetting of porous substrates by liquids, the liquid imbibition into porous layers and concomitant transport processes is important for many industrial applications, including ink-jet printing, 3D-printing, penetration of rain drops into building walls, needleless injection, coating of porous materials, irrigation, cooling of electronic devices. Recently, the interest to interaction of liquids with porous and textured surfaces has been increased, since they are promising as superhydrophobic and superamphiphobic surfaces [1,2].

Wetting of porous layers and imbibition are complex processes depending on the physical and chemical properties of the solid and the liquid, the geometry of the porous structure and the thickness of the layer [3]. The phenomena taking place during droplet spreading over porous media are schematically represented in Fig. 1.

Depending on the properties of the substrate and the liquid, droplets over porous layers may display different types of behavior, including non-wetting behavior, spreading over the surface of porous layer, as well as vertical and lateral imbibition into the layer. The interaction between the liquid and porous substrate is generally governed by dynamic wetting [4] and imbibition [5–7], which are often competing processes, with their relative importance determined by the relation of the respective time scales. If the porous medium includes nanoscale pores or nanoparticles, the influence of conjoining/disjoining pressure plays an important role [8]. If the liquid spreading over a porous layer is volatile, evaporation may bring about additional effects significantly changing the wetting state [9,10]. If the drop hits the substrate with a non-zero velocity, the liquid penetrates into the pores by inertia. The velocity of the dynamic pore filling may significantly exceed the impact velocity, if the pore size is much smaller than the droplet size [11,12]. Additionally, the flow of liquid through the porous layer not supported by impenetrable substrate can be induced by mechanical pumping [13].

Lateral imbibition may take place not only in porous layers, but also on rough or textured surfaces which can exert a capillary action [14]. Typical structures of porous or textured layers which are encountered in practice or used as model surfaces in research are schematically represented in Fig. 2. In Fig. 2a an isotropic open-porous structure is presented. A structure comprised of spherical particles is shown in Fig. 2b. This structure is also isotropic. In Fig. 2c a substrate containing cylindrical unidirectional non-interconnected pores is represented. This is evidently an anisotropic structure which of course does not allow any lateral imbibition (imbibition in the direction normal to the pores axes). A substrate decorated with cylindrical pillars is shown in Fig. 2d. Finally, a substrate coated by a (nano)fiber mat (fibers aligned parallel to the substrate plane) is shown in Fig. 2e. This structure possesses significantly different transport properties in direction parallel to the fibers in comparison with the properties in normal direction.

Porous media and porous layers can be classified according to their saturation with penetrating liquid. In dry porous media the whole pore volume is filled with air, in saturated porous media all pores are filled with liquid, and, finally, in partially saturated porous media,

E-mail address: gtatiana@ttd.tu-darmstadt.de.

http://dx.doi.org/10.1016/j.cocis.2014.09.001
1359-0294/

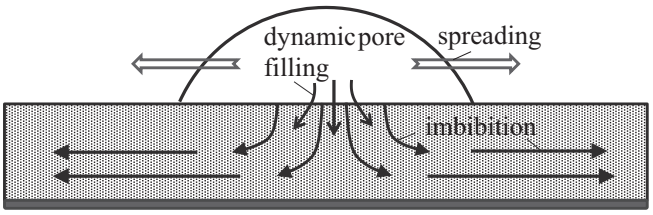

Fig. 1. Schematic representation of phenomena taking place during a droplet spreading over a porous layer.

some of pores are filled with liquid, or, alternatively, some pores are partially filled. In the partially saturated porous media the liquid can constitute isolated areas or a percolating network.

Heat and mass transport during spreading and imbibition of liquid droplets bring new degree of complexity and new time scales into the process. Numerous technically highly relevant processes, such as heat transfer enhancement by using structured or porous substrates, or transport and deposition of particles or caring substances onto fabric fibers, depend on wetting and imbibition hydrodynamics. At the same time the transport processes may influence the hydrodynamics of wetting and imbibition.

The present review discusses the progress in experimental and numerical studies of wetting and imbibition of porous media, layers and coatings (Section 2.1) and the relevant processes on the scale of a single pore or fiber (Section 2.2). Detailed knowledge of the micro- and nanoscopic processes taking place on the scale of single elements or element groups of the porous structure is necessary for understanding of wetting, imbibition and transport processes on the macroscopic scale. In some of the works presented in Section 2 evaporation plays a certain role in fluid transport. Section 3 is devoted to heat transfer and phase change, especially for cooling applications. Since the investigations of heat transfer coupled with wetting of porous layers are relatively rare (although extremely promising for heat transfer enhancement), several works dealing with the heat transfer enhancement on textured surfaces have been included into the review. Discussion of these works helps to elucidate the physical mechanisms affecting heat transfer enhancement and to identify the existing unresolved issues. Section 4 is devoted to a brief review of works on particles deposition accompanying wetting of porous media and some further applications. A special focus is laid on (nano)fibrous materials. The review is concluded by a brief summary and a suggestion of focuses for the future research (Section 5). The influence of surfactants on the spreading process and the effect of fluid mixtures are beyond the scope of the present review.

2. Wetting and imbibition

2.1. Porous media, layers and coatings

In the Subsection 2.1.1 the physics of imbibition is briefly discussed. After that wetting states which can be observed on porous or textured layers are described and discussed (Subsection 2.1.2) with a focus on mechanisms forcing the liquid penetration into the layer in the cases where the liquid initially does not penetrate spontaneously into the porous structure. Subsection 2.1.3 is devoted to discussion of simultaneous spreading and imbibition of liquid droplets into porous layers and coatings.

2.1.1. Physics of imbibition

The simplest case of imbibition is a spontaneous liquid penetration into a cylindrical capillary tube brought in contact with a liquid pool (Fig. 3a). It is assumed that the tube diameter is smaller than the capillary length $\sqrt{\gamma/(\rho g)}$, where γ is the surface tension, ρ is the density of the liquid and g denotes the acceleration of gravity. The capillary length for water at a room temperature at terrestrial conditions is around 2.7 mm. Apart from the initial and the final stages of imbibition, the dynamic of this process is governed by the balance between the capillary and viscous forces. The capillary pressure at the liquid-gas interface is given by the expression $p_c = \gamma \cos\theta/a$, where θ is the equilibrium contact angle and a is the inner radius of the tube. The Poiseuille parabolic velocity profile can be assumed for the flow in the tube far from reservoir. The average liquid velocity can be computed from the following relation:

$$u_{av} = \frac{\mathrm{d}l}{\mathrm{d}t} = -\frac{\partial p}{\partial z}\frac{a^2}{8\mu} = \frac{\gamma\cos\theta}{l}\frac{a}{8\mu}, \tag{1}$$

where l denotes the meniscus height and μ is the dynamic viscosity of the liquid.

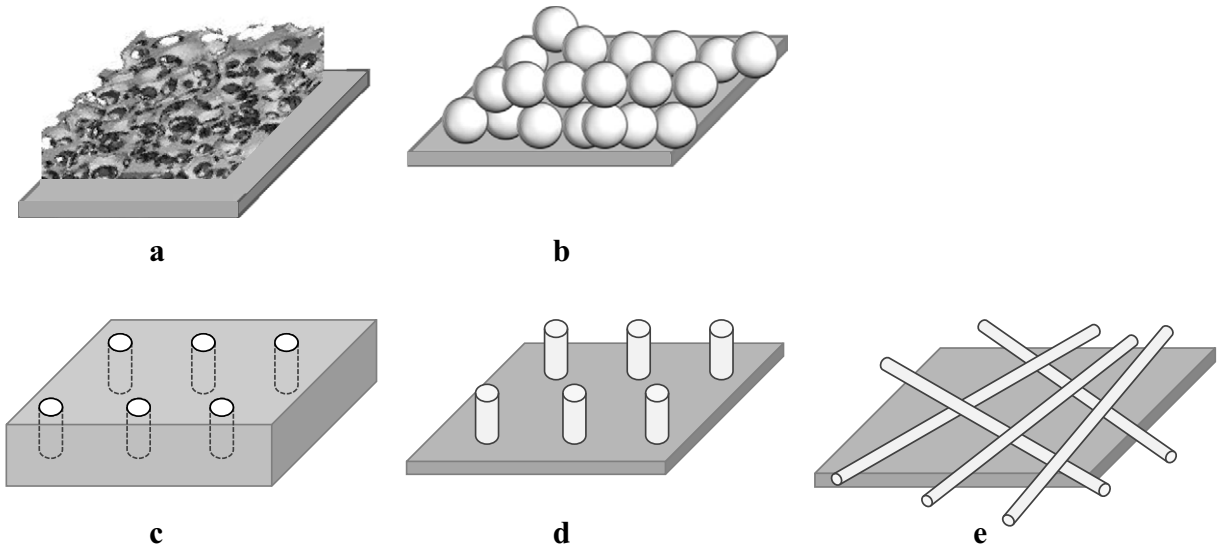

Fig. 2. Schematic representation of porous structures. (a) Isotropic open-porous structure; (b) isotropic structure comprised of spherical particles; (c) anisotropic porous structure with pores in the form of straight channels without interconnection; (d) array of pillars; (e) fiber mat.

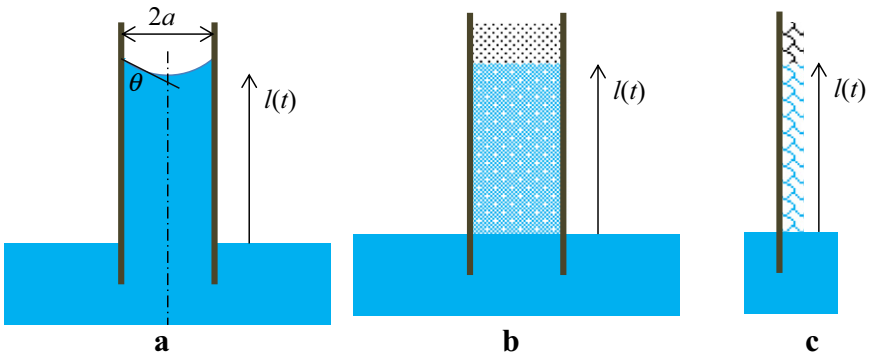

Fig. 3. Schematic representation of liquid imbibition from a reservoir into (a) capillary tube, (b) porous media, (c) substrate coated with porous layer or rough/microstructured substrate.

Integration of this equation leads to the Washburn law [5,15–17]:

$$l = \sqrt{\frac{\gamma a \cos\theta}{2\mu} t}. \tag{2}$$

One of the consequences of this diffusion-type relation is that imbibition into a circular tube occurs only for wetting liquids: $0 < \theta < 90°$.

Eq. (2) is not valid at the early stage of the imbibition process, when the process is inertia-dominated (at $t < \rho a^2/\mu$). At very short times the penetration velocity is constant and equal to $\sqrt{2\gamma\cos\theta/(\rho a)}$ [16,18]. Additionally, if the tube is oriented vertically, gravity affects the force balance at the latest stage of imbibition. The effect of gravity results in deceleration of imbibition dynamics until the meniscus stops at an equilibrium position. Eq. (2) is also not valid if liquid penetrates into a tube from a droplet instead of infinite reservoir [19]. In this case the Laplace pressure of the droplet should be taken into account in the force balance.

The $\sqrt{t}$ – dependence of capillary rise can be also observed for surfactant-induced imbibition in hydrophobic capillaries in the case where the diffusion of surfactant is a rate-determining phenomenon [20]. Of course, the physical mechanism leading to this dependence is very different from that underlying the Washburn law.

The imbibition of liquid into an initially dry porous column (Fig. 3b) follows the same time dependence as the imbibition into a capillary tube. Indeed, assume that the flow in the porous medium can be described by the Darcy's law:

$$\boldsymbol{u} = -\frac{1}{\mu} K \nabla p, \tag{3}$$

where $\boldsymbol{u}$ is the filtration velocity (volumetric flow rate in direction of pressure gradient divided by the cross-sectional area) and K is the permeability of porous material. It follows from continuity equation that the pressure field satisfies the Laplace equation. For one-dimensional flow this means that the pressure varies linearly with the length. The imbibition velocity is given by $\frac{dl}{dt} = \frac{Kp_c}{l\mu\phi}$, where ϕ denotes the material porosity. The impregnation length computed by integration of this equation is given by

$$l = \sqrt{\frac{2Kp_c}{\mu\phi} t}. \tag{4}$$

Herein the capillary pressure contains information about the material wettability, the typical pore size and shape.

Another important example is imbibition of liquid into a porous layer covering a solid substrate or imbibition into a rough, micro- or nanotextured substrate, which can exert a capillary action (see Fig. 3c) [11,14,17,21]. Bico et al. [14] developed a model for the condition of liquid imbibition into the texture. According to [14], imbibition takes place if the contact angle is below a critical contact angle θ_c, such that

$$\cos\theta_c = (1-\phi_s)/(\phi_s - r). \tag{5}$$

Herein r denotes the roughness, which is a ratio of the actual surface area to the projected area of the rough/microstructured substrate, and ϕ_s denotes the ratio of the solid area remaining dry (for example, the top surface of the micropillars) to the projected area. The critical contact angle for imbibition is always below 90° and depends on the properties of microstructure/roughness. A substrate coated with a porous layer can be considered as a limiting case of a rough/microstructured substrate with the roughness r approaching infinity, leading to $\theta_c = 90°$. If the condition of imbibition is fulfilled, [14] predicts that the time evolution of imbibition front along the solid substrate obeys the Washburn law ($\sqrt{t}$ – dynamics). Experiments performed on a textured surface (regularly spaced micro-size spikes) coated with octadecyl thrichlorosilanes validate this prediction [14].

Of course, the integral characteristics of the porous medium, such as the average material permeability, do not take into account the local microstructure of the substrate, which governs the local position of the contact line and, therefore, affects the imbibition process. One of the manifestations of the role of detailed microstructure is the anisotropic imbibition. The anisotropy of imbibition has been observed for a microstructure comprised of square array of micropillars with a radius of 25 μm, a height of 60 μm and a pitch of 100 μm attached to a solid substrate (similar to texture illustrated in Fig. 2d) [17]. Namely, the velocity of the imbibition front propagation was different in direction parallel to the side of the square array compared to the front propagation along the diagonal. As a result, the substrate area impregnated with the liquid took different shapes, including square and octagonal.

2.1.2. Role of wetting states and wetting transition

Consider simultaneous wetting of porous or micro- or nanostructured layer by an impacting or gently deposited liquid droplet and the imbibition of liquid into the layer. This process is different from the liquid imbibition from an infinite reservoir illustrated in Fig. 3. First, in this situation the liquid reservoir (droplet) has a finite volume, which affects the long-time wetting and impregnation dynamics. Second, the conditions of liquid penetration into the porous/structured layer, which are necessary for the imbibition process, are different in configuration illustrated in Fig. 1 compared to the situation illustrated in Fig. 3c, especially if the microgeometry of the layer is anisotropic. When a liquid droplet comes into contact with a porous, rough or textured substrate, several wetting states can be distinguished [15]: (i) Cassie-Baxter state, in which the liquid does not penetrate into the pores/cavities, and the droplet is partially supported by the solid and partially by air [22]; (ii) Wenzel state, in which the liquid completely wets the pores directly under the droplet [23]; (iii) Cassie-Baxter impregnating wetting state,

in which the liquid wets the pores/cavities not only directly under the droplet, but also ahead of the contact line. In addition, mixed states have been observed, in which the liquid only partially penetrates into the pores and cavities. The stable Cassie-Baxter state is characterized by large contact angles. The apparent contact angle in this state is usually computed using the Cassie-Baxter equation:

$$\cos\theta_{app} = \phi_{sl}\cos\theta - (1-\phi_{sl}), \tag{6}$$

where ϕ_{sl} denotes the ratio of the liquid-solid contact area to the projected area. The Cassie-Baxter state is a necessary condition for superhydrophobicity [10,15,24]. In the Wenzel state the apparent contact angle θ_{app} is usually computed using the well-known Wenzel equation:

$$\cos\theta_{app} = r\cos\theta. \tag{7}$$

This means that the apparent contact angle on textured/porous surfaces made of hydrophilic material is lower than the intrinsic (Young) contact angle θ, whereas the apparent contact angle on a surface of hydrophobic material is larger than θ. For the case of substrates coated with a porous layer, the pure Wenzel state is typical for anisotropic porous media constituted of bundle of capillary tubes oriented normal to the substrate, with no interconnection between the pores [25–28]. The Cassie-Baxter impregnating wetting state corresponds to the classical imbibition (normal and lateral) into the porous layer.

It can be expected that the Cassie-Baxter state is characteristic for substrates with $\theta > 90°$. Indeed, artificial superhydrophobic substrates are often manufactured as very rough or textured surfaces containing topographical features at different length scales. These surfaces are made of inherently hydrophobic materials [29] or coated to ensure a Young contact angle above 90° [1,30]. However, it has been predicted [2] and observed [11,15,31] that the Cassie-Baxter state is possible for inherently hydrophilic materials. These states are metastable and are usually observed for the textures, on which the incremental replacement of solid-air interface with solid-liquid interface during the filling of cavities and concomitant reduction of the surface energy is overcompensated by the growth of the energy of the liquid-gas interface which is increased during the filling of cavities [15]. This situation is typical for textures containing re-entrant pores.

The Cassie-Baxter state has been observed for substrates covered with nanofiber mats electrospun from poly(acrylonitrile) (PAN) solution [11]. The water contact angle on a cast sample of this polymer is around 30-40°. The mat used in [11] had a thickness of 200 μm and a porosity of about 90-95%. The fibers having a diameter of several hundreds of nanometers were arranged parallel to the substrate plane (as in Fig. 2e). The advancing contact angle measured for a millimeter-size water droplet gently deposited on the nanofiber mat surface was 103°. This contact angle is significantly higher than the inherent contact angle of the polymer. This indicates that the droplet is in a Cassie-Baxter state and is partially supported by the fibers and partially by the air. The existence of this metastable state is evidently a result of the specific porous structure formed by the assembly of nanofibers.

The wetting state can be changed. The wetting transition (change of wetting state) is accompanied by an abrupt change of an apparent contact angle [15]. The transition from Cassie-Baxter to Wenzel state or from the classical Cassie-Baxter to Cassie-Baxter impregnating wetting state (associated with lateral imbibition) can be triggered by impact of a droplet [11,32], compression [29], evaporation [10,24,33], mechanical vibration and active mechanical suction of liquid [13].

In [11,12] the transition from the classical Cassie-Baxter state to Cassie-Baxter impregnating wetting state has been observed for PAN nanofiber mats of the thickness varying from 100-200 μm to about 1 mm during impact of water droplets with the velocity V_d of the order of 1-2 m/s. The optical characterization of the impregnation area was possible for relatively thin mats, since the impregnated part of the mat had different optical properties compared to the dry part. The evolution of diameter of the imbibition region was determined by detection of the mat area which appeared darker than the dry nanofiber mat. In [11] the drop impact experiments have been performed at room temperature. In [12] the wetting transition has been observed on electrically heated stainless steel foils coated with nanofiber mats. The initial temperature of the foils varied in the range between 60 °C and 120 °C. The transient temperature distribution at the back side of the stainless steel foil has been measured using infrared thermography. It has been found that at every time instant after the droplet impact the imbibition region coincided with the region with reduced temperature. Therefore, the radius of the imbibition zone could be deduced not only by optical observations, but also from the temperature field. In [11,12] the wetting transition and water imbibition were registered for all tested drop impact velocities and all nanofiber mat thicknesses. It has been suggested that the mechanism of wetting transition for water droplets on PAN nanofiber mats was the inertia of impact forcing the liquid into the pores. A penetration velocity of the order of $V_d D_d/a^* \gg V_d$ has been predicted, where a^* is a characteristic pore size. The high penetration velocity has been explained by accumulation of the droplet kinetic energy by passing the liquid through narrow pores. However, the hypothesis of wetting transition mechanism triggered by impact was not tested by direct measurements in [11,12].

The liquid penetration into and through a free nanofiber layer (membrane) induced by impact has been systematically studied in [32]. In this work four polymers with different surface energy have been used for the manufacturing of nanofiber mats. Water, fluorinert fluid FC 7500 and hexane have been used as test fluids, which allowed variation of the surface tension and viscosity. The thickness of the nanofiber mats was also varied. At low velocities of the droplet impact onto the mats the outcome of impact (penetration, retraction) depended on the wettability. However, as the impact velocity became high enough, the liquid penetrated through the mat and formed a large droplet (water) or several jets (low surface tension liquids) on the back side of the membrane. The penetration was achieved even for the water drop impact onto the superhydrophobic Teflon nanofiber mat. The critical impact velocity of penetration was shown to be an increasing function of the mat thickness. The authors estimated the maximal mat thickness which can be penetrated by a droplet as $h_{max} = \rho V_d a^{*2}/\mu$. This means that the impact-driven penetration of liquid into porous medium at relatively high impact velocities is determined by the competition between the inertia and viscous forces. It is evident that the droplet impact would lead to the wetting transition at any textured superhydrophobic substrate, independent from the surface tension or wettability, provided the impact velocity is high enough. For water droplet impact with a velocity of $V_d = 1$ m/s and the estimated pore size of $a^* = 10$ μm in the mat the maximal mat thickness for penetration is $h_{max} = 100$ μm. However, the results reported in [12] indicate that the wetting transition takes place for the nanofiber mat thicknesses one order of magnitude higher than 100 μm. This means that, in addition to the impact, further mechanisms may be responsible for the wetting transition.

Transition from the Cassie-Baxter state to the Wenzel state or to Cassie-Baxter impregnating wetting state and breakdown of superhydrophobicity can be induced by evaporation of droplet [10,24,29,33,34]. As the droplet size decreases due to evaporation on a surface with low contact angle hysteresis, the curvature radius of the concave droplet-gas interface decreases. The curvature radius of the liquid-gas interface on the drop side adjacent to the porous/textured substrate decreases as well, so that mechanical equilibrium is maintained. This leads to the partial penetration of the liquid into the pore (or into the area between the pillars). As the curvature reaches a critical value, the local contact angle at one of the pinning points of the liquid-solid interface exceeds the advancing contact angle. As a result, the contact line depins, and the liquid slides into the pore or cavity.

The above wetting transition scenario has been directly observed by Moulinet and Bartolo [33]. They followed the evolution of the liquid-gas interface shape under a water droplet (initially at a fakir state) using the reflection interface contrast microscopy (RISP). This method allows a three-dimensional reconstruction of the interface shape. The superhydrophobic surface used in experiments was a poly(dimethylsiloxane) (PDMS) surface decorated with cylindrical pillars arranged in a triangular array with a pitch of 50 μm. The radius of the pillars was around 10 μm, and the height was 13 μm and 9.5 μm for different surfaces. The authors measured the depth of liquid penetration into the texture at different stages of drop evaporation. They found that the dependence of penetration depth on the drop radius (or, equivalently, on the Laplace pressure) was rather weak until the contact line depinning from a pillar edge at a certain location of the substrate took place. The depinning event leads to the wetting transition.

Qualitatively similar processes have been monitored by Papodopoulos et al. [10] for water droplets on glass substrates decorated with cylindrical PDMS pillars and SU-8 photoresist pillars with a square cross-section. The Laser Scanning Confocal Microscopy (LSCM) made it possible to visualize the three-dimensional shape of the liquid-gas interface under the droplet. Depending on the distance between the pillars in the square arrangement, two different scenarios of the wetting transition during droplet evaporation have been observed. The wetting transition through depinning, similar to that reported in [33], has been observed at relatively small distance between the pillars (40 μm for the pillar height of 23 μm). At larger interpillar distances (200 μm for the pillar height of 23 μm) the wetting transition via sagging has been observed. In this regime the depth of liquid penetration between the pillars increases in the course of droplet evaporation until it becomes equal to the pillar height. The local contact angles at the pinning edges are at this instant still below the advancing contact angle. The wetting transition occurs as the liquid-gas interface touches the substrate.

In [35,36] spontaneous transition from the Cassie-Baxter state to the Wenzel state is visualized for water droplets on substrates with square arrays of 10 μm-high pillars having a square cross-section. The intrinsic contact angle of the substrate material (based on the "kraton" block copolymer) is 100°, whereas the apparent contact angle for the microstructured substrate in the Cassie-Baxter state is 160°. The authors have evaluated the energy gain during wetting of a small portion of microstructured hydrophobic wall after an initial spontaneous local breakdown of the Cassie-Baxter state. As a result, a critical value of intrinsic contact angle θ_c has been derived, at which the energy gain is equal to zero. If the intrinsic contact angle is below θ_c, then the filling of the gas pockets underneath the droplet takes place. The critical contact angle increases with increasing of the distance between the pillars at a constant pillar height. Interestingly, if the intrinsic contact angle is below but close to θ_c, a square-shaped wetted area is developed, which is explained by so-called zipping mechanism of the air pockets filling, in which wetting of a new row of pillars starts after the previous row of pillars is wetted [35,36]. In spite of different mechanisms involved, the anisotropic growth of wetted area under the droplet resembles the anisotropic imbibition of liquid into a substrate decorated with a periodic array of micropillars [17] (see Subsection 2.1.1).

Several theoretical-numerical works have been devoted to prediction of Cassie-Baxter to Wenzel transition. Emami et al. [37] developed a numerical model for description of equilibrium position of water-air interface in electrospun thin coatings with porosity of 70% to 90% exhibiting superhydrophobic behavior. The simulations have been performed for the nanofibers with diameters in the range from 100 nm to 500 nm made of intrinsically hydrophobic material (contact angle ranging from 100° to 120°). The nanofibers were assumed to be arranged parallel to the wall. To simplify the model, the authors assumed that fibers behaved as sharp edges on which the liquid-air interface was pinned. Moreover, it was assumed that the liquid-air interface touched all fibers of the (thin) coating. The interface position depending on the applied pressure was computed by solving an integro-differential equation describing the force balance. A special focus has been laid on prediction of the pressure corresponding to transition from the Cassie to Wenzel state. According to the model, the depinning of contact line and wetting transition occurred as soon as the angle between the meniscus and the fibers reached a prescribed contact angle. The typical predicted values of transition pressure were 20–60 kPa, with higher transition pressures predicted for coatings with nanofibers arranged in ordered orthogonal meshes in comparison with chaotically oriented nanofibers. This range of transition pressures corresponds to capillary pressure in a droplet with a radius of the order of micrometer, which is comparable with the size of inter-fiber pores. The results of [37] imply that the wetting transition induced by evaporation and depinning observed for substrates decorated with pillars [10,33] is not feasible for nanofiber-coated surfaces.

2.1.3. Simultaneous spreading and imbibition

In Subsection 2.1.3.1 an overview of experimental works on simultaneous spreading of liquid over porous layers and imbibition is given. The theoretical and numerical works are reviewed in Subsection 2.1.3.2.

2.1.3.1. Experimental works. Several experimental studies of simultaneous spreading of droplets over porous media and imbibition are described in [38–40] and reviewed in [41]. The typical droplet behavior on porous layers can be subdivided into three phases: (i) initial, relatively fast droplet expansion, governed mainly by the forces outside the porous substrate, (ii) pinning of the contact line at the maximum reached spreading diameter and the contact angle decreasing due to the volume loss in the drop caused by the imbibition, and (iii) the shrinkage of the drop base at almost constant apparent receding contact angle. In some systems the pinning phase does not take place [39]. Typically the main outcome of experimental observations is the evolution of the droplet base radius (the radius at the contact with the substrate), the evolution of size (and shape) of the wetted region of the porous medium (if the medium is initially dry) and the evolution of apparent contact angle at the droplet base. The data are sometimes represented in the form of evolution of the droplet volume over the substrate.

Starov et al. [39] studied the spreading of silicone oils with viscosities ranging from 0.02 kg/(m s) to 0.6 kg/(m s) over initially dry thin cellulose nitrate membrane filters with pore sizes of 0.2 μm and 3 μm, porosity ranging between 65% and 87% and thickness around 130 μm. The initial droplet volume was varied between 3 mm^3 and 15 mm^3. The static receding contact angle for silicone oils on non-porous substrate is equal to zero (complete wetting) [41]. In this system the initial stage of drop expansion took a very small fraction of the time needed for total imbibition and disappearance of droplet. After reaching the maximal droplet base radius the drop started to shrink without any pinning period. The most important result of the experiments was the universal time dependence of droplet base radius, radius of wetted area in the porous medium, and the apparent contact angle. In the universal time dependence the imbibition time $t_p^* = \frac{l_m^2 \mu \log\left(l_m/R_b^*\right)}{K_p p_c}$ has been used as a time scale, where l_m denotes the maximal radius of the wetted area in the porous layer (which can be easily computed using the mass balance and assuming that the drop is totally imbibed), and R_b^* is the characteristic droplet contact radius. The product $K_p p_c$ has been determined independently by experiments on imbibition of liquid from a large reservoir into a vertically arranged membrane (by comparing Eq. 36 from [39] with Eq. (4) of the present work it can be concluded that $K_p = K/\phi$). The apparent contact angle determined by the hydrodynamics of the process stays constant during the shrinkage stage.

As soon as spreading/imbibition experiments are performed on a thick porous medium instead of a thin membrane, the universal character of droplet radius evolution breaks down if substrates with different porosities and different pore sizes are tested [40,41].

Spreading and imbibition of partially wetting liquids (water) over the same membranes tested in [39,41] is characterized by a long period of contact line pinning at a maximal droplet spreading (more than 60% of the total time of spreading/imbibition). The duration of the pinning phase could be shortened by addition of an anionic surfactant.

Clarke et al. [42] studied spreading of water droplets and droplets of aqueous solution of glycerol and hexelene glycol (viscosity 0.04 kg/(m s), surface tension 0.038 N/m) over membrane filters made from cellulose esters with estimated mean pore diameters varying between 0.1 μm and 0.8 μm and porosity varying in the range 74% to 82%. The authors recorded the evolution of the droplet volume (over the substrate) in time. They did not follow the size of the imbibed region. It was assumed that the transport of liquid into the porous structure took place mostly vertically (normal to the substrate). In all experiments the rate of decrease of droplet volume (rate of imbibition) increased with increasing of the average pore size (in a qualitative agreement with the Washburn's law for a capillary tube, Eq. (2)). After the short spreading phase the water droplets stayed pinned at the maximal spreading diameter, whereas the droplets of solution having a lower surface tension did not pin. This difference in behavior is in a qualitative agreement with the experimental results reported in [39,41]. The experiments [42] revealed a striking discrepancy in characteristic time of imbibition between the water and the aqueous solution of glycerol and hexelene glycol. The imbibition of solution which has lower surface tension but much higher viscosity than water takes place 4 orders of magnitude faster than imbibition of water. The slow imbibition of water can be attributed to delay in water penetration into the pores due to poor wettability. The authors measured the apparent contact angle for water droplet over a membrane filter. The apparent contact angle varied between 51° and 83°. However, no data on contact angle for a non-porous substrate of the same material were reported in the work.

Direct visualization of the liquid distribution in the porous medium during the droplet imbibition process is a very challenging task. In [43] the drop spreading and penetration has been visualized, and the evolution of the penetration depth and width of the wetted region in the porous substrate has been quantified. The artificial porous substrate was prepared from transparent glass beads, with three groups of beads used for different experiments: small beads (70–110 μm), medium beads (150–300 μm) and large beads (420-590 μm). The porosity of the medium was equal to 36% for all cases. The experiments have been performed with water and with mixture of toluene and diiodomethane. Using this mixture made it possible to match the refractive indices of the liquid and the glass beads. The visualization of the droplet impact and imbibition is presented in Fig. 4. The process captured by these four images takes 10 ms. The bright regions within the porous medium correspond to the area filled with the liquid. The evolution of depth and width of the wet region in the porous medium has been recorded after drop impact, where the droplet diameter varied between 1.55 mm and 3.2 mm, and the maximal impact velocity was 5.32 m/s. It has been found that for the impact velocity below 3 m/s the evolution of the penetration depth and width are independent from the impact velocity and are therefore dominated by the capillary forces. At low impact velocities the penetration depth was very well predicted using the Washburn's approach. To derive the evolution equation for the liquid front in the porous media, the Darcy's law (Eq. (3)) has been applied with the permeability evaluated using the Carman-Kozeny expression. The average capillary pressure at the wetted/dry interface (required for evaluation of the pressure gradient in the Darcy's law) has been computed using the relation

$$p_c = \frac{2\gamma(1-\phi)}{D_b\phi}(2\cos\theta + \sin\theta), \tag{8}$$

where D_b is the average bead diameter, and θ is the instantaneous velocity-dependent contact angle. It has been shown that for the experimental conditions the dynamic effects of wettability, namely, the dependence of the dynamic contact angle on the propagation velocity is significant and has to be taken into account.

Grzelakowski et al. [28] studied experimentally the influence of pores topology on free imbibition of sessile droplets into nanoporous membranes. The test liquids were non-volatile PDMS oils with viscosities of 1 kg/(m s) and 5 kg/(m s) and a surface tension of 0.02 N/m. The experiments have been performed on two sides of a nanoporous alumina membrane with gradient porous structure, so that one side of the membrane had a structure consisting of straight parallel channels with average diameter 250 nm, and the other side had a porous structure consisting of interconnected channels of average diameter 90 nm. The surface fraction of the pores has been identical from both sides and equal to 46%. The wetting and imbibition have been studied by placing the droplets of PDMS oil on either side of the membrane and observation of the droplet size and shape evolution. It has been found that the droplet spreading diameter evolution on the nanoporous membrane follows the power law with the scaling exponent below 1/10. The Hoffman-Voinov-Tanner law predicts that the radius of a thin droplet spreading over a non-permeable surface increases as $t^{1/10}$ [4]. Therefore, the drop spreading over a porous layer is retarded in comparison with a non-permeable wall. This spreading retardation has been attributed to the competition between spreading and imbibition. In addition, it has been observed that the spreading is notably faster on the membrane side with small and interconnected pores, which indicates that imbibition rate into porous structure with small interconnected pores is lower than that with straight larger pores. According to the Washburn's law for imbibition into a capillary tube (Eq. (2)) and in agreement with the experiments in [42], the one-dimensional imbibition rate is expected to be higher for larger pores (at the equal surface area fraction of pores). Therefore, the higher imbibition rate for smaller interconnected pores can be explained by the lateral imbibition of the liquid.

Leese et al. [26] have studied experimentally the wettability of nanostructured porous anodic alumina as a function of the pore diameter for the constant porosity. The experiments have been performed for hydrophilic (bare anodic alumina) and hydrophobic (silanized) surfaces. The contact line of water droplet on a non-porous smooth hydrophilic surface was $12 \pm 2°$ and the contact line on a non-porous silanized surface was $103 \pm 2°$. The porous structure was comprised of holes with nearly cylindrical shape which were not connected with each other and which were bounded from one side by an impermeable substrate. In this

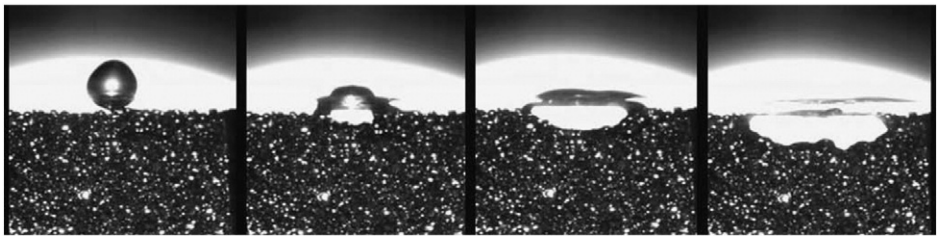

Fig. 4. Drop impact onto a porous substrate (reproduced from [43]).

configuration there exists a final equilibrium state of non-volatile droplets which can't completely imbibe into the porous layer due to the finite available volume of the (not interconnected) porous space and due to air entrainment in the pore under the meniscus created at the bottom side of the drop. Because of geometrical constrains, the air can't escape from the pore when the drop is placed over the substrate. The entrained air exerts a pressure upon penetrating liquid thus affecting the equilibrium shape of the drop and the apparent contact angle. It has been found that the equilibrium apparent contact angle of the droplet is a strong function of the pore diameter. For the hydrophilic surface the equilibrium apparent contact angle for water droplets increased from 13° to 100° for the pore diameter changing from 10 nm to 170 nm. For the hydrophobic surface the equilibrium apparent contact angle increased from 106° to 150° with increasing of the pore diameter from 10 nm to 170 nm. Since the apparent contact angle is a function of the pore size, the classical Cassie-Baxter Eq. (6) is inapplicable. Singh et al. [44] found out that the nanoporous structure of the anodic alumina and the pore size significantly affect not only the wettability and the transition from Cassie-Baxter to Wenzel state but also the evaporation dynamics of drops.

Recently rising attention of researchers is attracted to the drop behavior on nanofibrous porous layers. Such nanofiber layers currently can be produced by electrospinning. The interest in nanofiber coatings is supported by the simplicity, inexpensiveness and versatility of the nanofibers fabrication process. Li et al. [45] have shown that it is possible to control the wettability and mechanical properties of nanofiber mats by adjusting of the polymer solution chemistry in electrospinning process. Wang et al. [46] have demonstrated that a drop gently deposited on a superhydrophilic fibrous mesh with nanochannels spreads extremely fast, with the velocity of order of magnitude 0.25 m/s. On the other hand, a partially wettable nanofiber layer apparently behaves like a superhydrophobic substrate when a droplet is very accurately put in contact with it [11], as discussed in Subsection 2.1.2. The droplet base diameter doesn't change after the first drop contact with the substrate, showing no spreading. If such droplet impacts the surface leading to wetting transition, the fast phase of inertia dominated spreading is followed by a slow liquid imbibition into the layer. The apparent wetted spot inside the porous layer is irregular. Its characteristic radius increases first as a square root of time, reaches the maximum and then starts to decrease due to the liquid evaporation on the nanofibers. It was demonstrated that the volumetric fraction of the liquid in the porous layer is not a step function, dividing the substrate domain onto a wet and dry regions, but a continuous function of space. The porous medium is partly saturated with the liquid. The evolution of the volumetric fraction is described well by the diffusion-like equation [47]. Qualitatively similar phases of droplet spreading, imbibition and evaporation have been observed for water droplets over heat-treated silica soot layers [48].

2.1.3.2. Modelling. In the most of existing models describing simultaneous spreading and imbibition, the initially dry porous substrate is subdivided into two regions: wetted (completely saturated with the liquid) and dry. The flow in the wetted region is typically modeled using the Darcy flow (Eq. (3)), where the dependence of the permeability coefficient on the pores geometry can be estimated using numerous empirical or semi-empirical formulae available in the literature. The driving force of the liquid flow associated with the imbibition process is the capillary pressure, estimated as $p_c = 2\gamma/a^*$, where γ is surface tension and a^* is the characteristic pore radius. The description of flow in porous medium is combined with the description of behavior of droplet above the porous medium. The most important ingredient of any model describing the droplet spreading is the specific model of the dynamic contact line behavior, which requires an assumption about the contact angle value, contact angle hysteresis and contact angle dependence on contact line velocity. In addition, a specific way to eliminate the singularity near the moving contact line [49] should be chosen.

One of frequently used model porous media is a medium similar to that shown in Fig. 2c, comprised of non-interconnected capillary tubes [25,27,50]. The imbibition into individual tubes can be described explicitly using the Washburn's law.

Davis and Hocking developed a model for spreading and imbibition of a drop on an initially liquid-saturated [51] and on initially dry [27] porous substrate comprised of very long vertical capillaries. The flow in each pore have been modelled using the balance between the pressure gradient and the viscous forces (analogous to analysis of Washborn [5]), whereas the hydrostatic pressure as well as the capillary pressure difference between the meniscus in the pore and between the drop surface have been taken into account. The inertial effects in the flow inside the porous substrate were ignored. In the case of initially dry substrate the authors have posed a slip boundary condition at the porous wall in order to eliminate the contact line singularity. The drop evolution was described using lubrication approximation (or long-wave theory [52]), which allows to formulate a single evolution equation for the droplet profile. This approach is applicable for low apparent contact angles. The authors imposed a condition of constant contact angle for the droplet spreading over the porous layer. Moreover, this contact angle is equal to the contact angle formed by the liquid on the solid walls of the pores. This condition significantly limits the direct applicability of the developed model, since the apparent contact angle is modified by the presence of pores and, according to experimental results, changes with time [38–41,53].

Clarke et al. [42] developed a model for droplet spreading over a porous layer. In this model the relation between the contact line velocity and dynamic contact angle derived from the molecular-kinetic theory for a poreless smooth solid is applied for description of droplet dynamics. Using this relation for porous solids, where the apparent contact angle is determined by the complex microscopic flow pattern around and into the pores, is hardly justifiable. However, the introduction of the dynamic contact angle was an important step forward towards the theoretical/numerical description of simultaneous droplet spreading and imbibition. It was assumed that the liquid penetrates the solid in normal direction (no radial liquid transport). The flow in porous medium was described by Darcy's law under an assumption that the pressure gradient in the porous medium is governed by the capillary pressure. Inertial effects during imbibition were not considered. The model was used to explain experimental data with aqueous solution of glycerol and hexelene glycol discussed in Subsection 2.1.3.1, whereas three independent parameters have been fitted: (i) combination of porosity, permeability of the porous medium and characteristic capillary radius; (ii) "friction parameter" entering the relation between the contact line velocity and dynamic contact angle; (iii) static advancing contact angle.

Zadražil et al. [50] introduced additional physical phenomenon affecting the spreading dynamics over porous media. They have simulated solidification of a droplet of melt over a cold porous medium. As many other investigators, Zadražil et al. used the model of porous membrane with pores arranged normal to the surface (Fig. 2c). In addition to the time scales of spreading and imbibition, the time scale of solidification came into play to affect the spreading/imbibition dynamics as well as the final shape of solidified body. The droplet and the wetted region of the porous substrate have been assumed to be thin, so that their dynamics could be described in the framework of the long-wave approximation.

To avoid the singularity of the moving contact line, Zadražil et al. [50] have used the concept of disjoining pressure. Disjoining pressure accounts for the intermolecular forces between the solid, liquid and the gas phase and is important in the vicinity of the three-phase contact line, where the film thickness is of order of hundreds of nanometers and below. The form of disjoining pressure as a function of a local film thickness determines the equilibrium contact angle for the droplet above the substrate. Disjoining pressure, depending on its functional form, modifies the solution for the liquid film distribution near the apparent contact line in such a way, that a thin adsorbed film is formed

ahead of this apparent contact line. The contact line itself is distinguishable as a small region (of continuous film) characterized by a very high positive curvature. The contact line sharply separating between the dry and wet parts of substrate does not exist in the solution, and thus the singularity of dynamic contact line is eliminated. In the case of liquid spreading over a smooth solid substrate the concept of a disjoining pressure has a clear physical meaning and, depending on the properties of liquid and solid, accounts for different kinds of intermolecular forces, including van der Waals and electrostatic forces [16]. In the case of a substrate with pores at the scale of several micrometers, introducing the effective disjoining pressure is a mathematical method to avoid the contact line singularity and to force a certain equilibrium apparent contact angle.

Hilpert and Ben-David [25] described the droplet spreading and imbibition into porous media comprised of parallel cylindrical pores arranged normal to the surface. The droplet has been assumed to have a shape of spherical cap. The authors have taken into account the influence of dynamic contact angle and contact angle hysteresis on these processes. Two different forms of the (apparent) contact angle vs. contact line velocity relations have been considered: a relation of Hoffman [54] and the Hoffman-Voinov-Tanner law:

$$\theta^3 - \theta_0^3 = c_t \frac{u_{cl}\mu}{\gamma}, \tag{9}$$

where u_{cl} is a contact line velocity, c_t is a constant and θ_0 is a static (advancing or receding, depending on the sign of u_{cl}) contact angle. In [25] the following stages (or phases) of the spreading/imbibition process have been considered: (i) an increasing drawing area phase characterized by increase of the droplet base radius, the apparent contact angle is larger than the static advancing contact angle; (ii) a constant drawing area phase, characterized by the constancy of the droplet base radius; the apparent contact angle is larger than the static receding contact angle and smaller than the static advancing contact angle; (iii) a decreasing drawing area phase characterized by decreasing of the droplet base area as the apparent contact angle falls below the static receding contact angle. The problem of the formulation adopted in [25] is the ambiguity of definition of static advancing and receding contact angles for porous substrates.

Frank and Perré [55] used the lattice Boltzmann method to study the spreading of a droplet over porous media comprised of parallel vertical pores with hydrophilic surface. The pores have square cross-section. In this study the liquid spreading and imbibition have been simulated on the scale of a single pore. The inertia has been taken into account (which is especially important at the initial stage of spreading and imbibition), and no assumption has been made on the shape of the drop. A constant intrinsic contact angle has been forced by imposing a certain density value at the wall notes. In [55] the simulations have been performed for the values of intrinsic contact angle of 36° and 70°. The simulations have been performed for the initial stage of droplet spreading and imbibition, so that the half of the simulation time corresponds to the inertial spreading regime. The simulations have shown that, when the contact line during spreading reaches a hole, the spreading first takes place over solid surfaces around the pores, which leads to fingering over the pore-free surface. The apparent pinning of the contact line at the pores has been attributed to the time required to wet all the surfaces of the pore and to form a complete meniscus. This process is believed to contribute to the retardation of the global spreading dynamics. However, it is not clear, if the code used in this study was able to describe a physical contact line pinning at the sharp edge of the pore which is a well-known effect [4]. Numerical simulations of Frank and Perré have predicted that an increase in intrinsic contact angle and increase in porosity leads to decrease in both the power-law exponent and the prefactor in the equation $R_b = Ct^{\alpha}$ describing the evolution of radius of droplet-substrate contact during the early spreading stage.

In several studies simultaneous spreading and imbibition of droplets over porous substrate allowing a lateral transport of liquid is modelled.

Starov et al. [39] developed a spreading/imbibition model of a thin porous membrane in a case of complete wetting (see the discussion of experiment in Subsection 2.1.3.1). A large discrepancy between the fast time scale of initial droplet spreading and slow time scale of the following complete imbibition of the droplet made it possible to consider these two processes independently. Additionally, it has been assumed that the drop is thin (exhibiting low apparent contact angle during spreading/imbibition) and has a shape of spherical cap except for a very small region near apparent contact angle. For the spreading process, a concept of effective lubrication parameter, depending on the porous structure, has been used in [39]. This parameter could not been determined directly and therefore played a role of adjustable parameter. For the description of the liquid transport in the membrane it has been assumed that the membrane was fully saturated over a whole depth at the locations of contact with the droplet, and that the Darcy flow in the membrane was one-dimensional. The resulting differential equation for the radius of the wetted area within the membrane had the following form:

$$\frac{dl}{dt} = \frac{K_p p_c}{\mu l \log(l/R_b)}. \tag{10}$$

Eq. (10) is generally applicable for the radial flow in thin membranes with sharp boundary between the fully wet and fully dry areas in the case if the ambient pressure boundary condition can be posed at the distance R_b from the origin of the polar coordinate system. Of course, Eq. (10) should be solved simultaneously with an equation (or a system of equations) describing the evolution of R_b, which depends on the behavior of the contact line. In the system considered in [39] an asymptotic treatment of the problem was possible in the imbibition phase. This asymptotic treatment, which was validated by comparison with experiment, was based on an assumption that the change of the droplet contact radius during the imbibition phase is determined by the change of the droplet volume at a constant apparent contact angle.

Alleborn and Raszillier [56] investigated theoretically and numerically spreading and imbibition of droplets on anisotropic layered porous substrates of finite thickness with impermeable bottom side. The anisotropy of the porous layer, expressed in a permeability tensor for the description of Darcy flow, is relevant for imbibition of droplets into textile fabrics and into nanofiber mat coatings with the nanofibers arranged parallel to the substrates. The authors assumed that a sharp wetting front separates the completely saturated region in the porous substrate from the completely dry region. The droplet spreading has been modelled in the framework of the long-wave theory (thin droplets with low contact angles), and the behavior of contact line has been modelled using the concept of disjoining pressure.

One of the regimes described in [56] is the preferentially radial imbibition caused by the low thickness of a layer with high permeability. The same trends can be expected in the cases where the permeability in the direction parallel to the surface is much larger than that in the direction normal to the surface. The results presented by Alleborn and Raszillier [56] for the droplet spreading over a thick layer with the anisotropy ratio 0.1 (normal to parallel) show that the preferential radial imbibition becomes important at the late stages of imbibition (when nearly the whole volume of droplet is absorbed by the porous medium).

Application of models which use the permeability of porous media and capillary pressure as model parameters [56] requires the knowledge of material-specific properties. Several works are devoted to modelling of imbibition-related properties of porous materials with defined micro- or nanostructure, for example, fibrous materials. Mao and Russell [57] developed a model for prediction of capillary pressure and the rate of liquid wicking in non-woven materials based on fiber orientation and distribution, fiber diameter and material porosity. Anisotropy of material is taken into account in the model. The analysis [57] is valid

only for situation where the fully dry areas of the material are separated from the areas fully saturated with liquid.

In the most of the theoretical and numerical works mentioned above the dry areas of the porous medium have been supposed to be separated from the fully saturated areas by a sharp wetting front. In [55] the existence of sharp wetting front is not assumed, but dictated by the specific pore geometry. However, a sharp boundary between saturated and dry areas within porous media does not always exist during the droplet imbibition process, especially if the porous medium is comprised of pores of different sizes and shapes [11]. Depending on the micro- or nanoscale geometry and the wettability, the porous medium can be partially saturated, i.e. the pores are only partially filled with liquid, or only a fraction of pores at a certain location is filled with liquid. In this case the transport of liquid in the porous media can't be described using the Darcy's law with constant material permeability. Continuum-based methods for modelling of two-phase flow in porous media rely on saturation-dependent relative properties of medium, such as permeability and capillary pressure [47,59]. These dependencies should be determined separately for different porous structures. Alternatively, the two-phase transport in porous media can be described using a capillary network model which is based on the micro-force balance at the liquid-gas interface [58]. The porous medium in this model is represented as a network of pores connected by throats. The capillary pressure and the local permeability is determined by the length and radius of throats, and the saturation of medium is determined by the saturation of pores.

Markicevic and Navaz [60] have studied the imbibition of a sessile droplet into porous media using the capillary network model. The spreading of liquid droplet was not considered in this study. It was assumed that a droplet with a certain volume had been placed over the porous medium. The contact radius was assumed to stay constant during the imbibition process which followed the droplet placement. The simulations performed in framework of the capillary network model allowed prediction of two-phase imbibition flows, in which the pores are not necessarily saturated at every point behind the wetting front. Markicevic and Navaz [60] considered two stages of imbibition: the primary stage, in which some part of the droplet is outside the porous media, and the secondary imbibition (or infiltration), in which the whole liquid is inside the porous medium. During this stage, small volumes of liquid are formed, which are separated from the other liquid. These separated parts increase in number and decrease in size with the time until a certain stationary state is reached, in which the flow is terminated. According to the simulation results, the distribution of liquid within the porous media depends on the droplet contact radius, the parameters of the model porous media and the "heterogeneity" of the media, i.e. the deviation of, say, the throat radius from the average value. One of the difficulties of validation of the above model is the establishment of relationship between the parameters of the model porous media and the real porous media tested in experiments.

2.2. Pores and fibers

Wetting of porous media, layers and coatings involve multiscale wetting phenomena, where the highest scale refers to the wettings of the outer surface of the layer exposed to the environment, and the smaller scales refer to the wetting of individual pores, fibers or small groups of pores/fibers. The wetting of the porous layer and penetration of liquid into it crucially depend on the wetting phenomena on the smaller scales.

Delbos et al. [61] have performed experiments on forced wetting of hydrophobic and hydrophilic glass capillaries by impact of droplets. The drop diameter was kept constant and equal to 2.5 mm, the inner radius of capillary tube was varied between 0.1 mm and 0.5 mm, and the maximal impact velocity was around 2.4 m/s. Several regimes of the tube impregnation have been identified, depending on the impact velocity, surface properties and the inner radius of the capillary. For the small impact velocities, the liquid is not impregnated into the hydrophobic capillary and fully sucked into the hydrophilic capillary. At high impact velocities a certain amount of liquid penetrates into the capillary and forms a slug, whereas the rest of liquid stays at the upper surface. This phenomenon has been observed for both hydrophobic and hydrophilic capillaries. Interestingly, the amount of the liquid in the slug is equal to the amount of the liquid in the droplet just above the capillary. For a constant impact velocity, the liquid penetrates hydrophobic capillaries of large radius and does not penetrate the hydrophobic capillaries having small radius. For example, the critical tube radius for liquid penetration at the impact velocity of 0.5 m/s is close to 0.2 mm. The authors estimated the threshold velocity for the liquid penetration into hydrophobic capillary tube using the balance between inertia, the capillary pressure at the top of the drop and the capillary pressure at the bottom of the drop. At zero impact velocity the condition of liquid penetration into a hydrophobic capillary of radius a reduces to the condition introduced by Marmur [19]: $R_d/a < -1/\cos\theta$, where R_d is the droplet radius.

Ding and Theofanous [62] have applied the diffuse-interface method to simulate the inertia-influenced dynamics of a drop after impact upon a hydrophilic substrate with a single capillary. The contact angle hysteresis has been taken into account in the model. Depending on the Reynolds number based on the radius of capillary and Weber number of impacting droplets, the authors identified following regimes of penetration: (i) complete penetration regime, in which the liquid has enough time (in comparison with the droplet spreading time) to enter the capillary (for $R_d/a = 5$ and the Weber number below unity this regime takes place for the Reynolds numbers below 25); (ii) partial penetration of liquid as a slug; and (iii) penetration with liquid reentry and bubble entrainment. In the last regime the lamella formed by droplet spreading over the capillary bounds back and enters the capillary, entrapping the gas existing in the capillary. In inertia-dominated regime (partial penetration of the liquid), the amount of the liquid in a slug penetrated into capillary comes from an upright liquid cylinder above the capillary, in quantitative agreement with the experimental data [61]. The authors have extended their simulations to a substrate with a row of parallel capillaries. This row plays a role of a model porous medium.

Yue and Renardy [63] have applied a phase field method to study the spontaneous penetration of a liquid droplet into an exposed cylindrical pore arranged normally to the substrate for the case where the droplet size is comparable with the diameter of the pore and the contact angle is above 90°. The initial velocity of the droplet is zero. The model does not take into account gravity, inertia and the contact angle hysteresis. The numerical model used in [63] describes the wetting of the inner surface of the pore and also the surface of the substrate. Therefore, the model is highly relevant to the penetration of droplet into porous media. The authors identify five different penetration/spreading regimes depending on geometric parameters and the static contact angle. It is shown that, in spite of the fact that the pore surface is hydrophobic, spontaneous drop penetration is possible, if the drop diameter is sufficiently small. Theoretical analysis, which has been performed in addition to numerical simulations, yielded threshold values of droplet radius for transition between different regimes as a function of static contact angle. Of interest is the transition between the "spreading/no penetration" regime, in which the liquid spreads over the surface but does not wet the inner part of the pore, and the "spreading/penetration" regime, in which both the substrate and the inner part of the pore are wetted by the liquid. The corresponding geometric configuration is shown in Fig. 5, with $\pi/2 < \theta < 3\pi/4$. In this situation the curvature radius of the droplet portion above the substrate, R_2, is equal to the curvature radius of the meniscus at the droplet bottom, R_1. The condition of the above regime transition and the contact line depinning from the pore edge is $R_d/a < -f(\theta)/\cos\theta$. The factor $f(\theta)$, which allows to distinguish between this inequality and the threshold condition in [19, 61], varies between 0.8 and 1 in the range $\pi/2 < \theta < 3\pi/4$.

The transition between the states studied numerically in [63] can be related to the evaporation-induced wetting transition discussed in

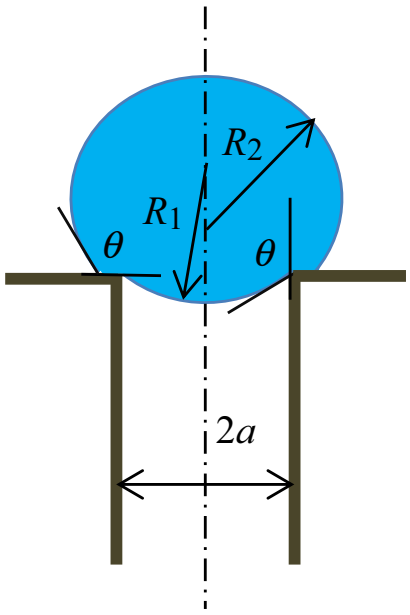

Fig. 5. Schematic representation of a droplet and a hydrophobic capillary. At this configuration under condition $R_2 = R_1$ liquid starts penetration into the capillary.

Subsection 2.1.2. However, neglecting the inertia not only precludes description of wetting transition triggered by impact, but also leads to erroneous predictions of penetration kinetics for $t < \rho a^2/\mu$.

In [64] the behavior of impacting droplet in the vicinity of a pore has been studied experimentally and numerically. Numerical simulations have been performed using the Volume-of-Fluid method, whereas inertia, viscous flow, wettability and surface tension have been accounted for. As in many other studies, a substrate with a group of isolated pores in the form of vertical channels with circular cross-section has been tested in experiment, and a single pore was used in simulations. The pore diameter was 1 mm, and the diameter of impacting droplets was 2.5 mm. The distance between the impact location and the pore was comparable with the droplet size. Both experiments and numerical simulations in [64] have shown that the expanding lamella created by the drop impact is disintegrated as it meets a pore. At high impact velocities, starting from about 3 m/s, the flow around the pore was accompanied by formation of jets. This phenomenon has been attributed to the impact of lamella flowing over a pore onto an opposite wall of the pore. This impact produced two jets: first directed upwards, and the second directed into the pore. The experimental and numerical results reported in [64] reveal new complex flow patterns pertinent to drop impact and spreading over a porous surface. These results make it clear that theoretical/numerical treatment of droplet spreading over porous substrates in the framework of classical models of wetting normally used for droplet spreading over flat solid substrates [25,27,42,50,51,56] is not justified.

Numerous experimental, theoretical and numerical works in the last two decades have been devoted to interaction of fibers with wetting liquids, with or without involvement of nanoscale effects. Neimark [65] developed a model describing the equilibrium shape of a droplet on a single nanofiber and derived an expression for a contact angle depending on the nanofiber diameter. This expression predicts a transition from partial wetting of carbon nanotubes by water to non-wetting at a fiber diameter 4.1 nm.

Static contact angles have been measured for external and internal surfaces of individual nanotubes using Wilhelmy force balance method [66,67]. It has been found that the static contact angle depends on the carbon nanotube diameter [66]. For example, the contact angle of glycerol for external surfaces of 20 nm diameter tubes was $77 \pm 2°$, and for the tubes with diameter of 60 nm the contact angle of $57 \pm 10°$ has been measured. The increased wettability at larger nanotube diameter was attributed to the higher number of defects. The experimental data indicate that for water the wetting of internal surfaces of nanotubes is characterized by smaller contact angles in comparison to external surfaces. Rossi et al. [68] studied the wetting of carbon nanotubes with diameter of 200–300 nm using environmental scanning electron microscopy. They observed menisci formed by condensation of water from the water vapor at a pressure of 4–6 Torr and temperature of 4–5 °C. The authors could observe water plugs inside the open nanotubes before the condensation at the outside of the tubes was visible. This behavior is in a qualitative agreement with the results presented in [66]. The estimated contact angle between the water and walls of nanotube was 5–20°.

Several works have been devoted to propulsion of droplets [69] or droplet size and morphology change [70] on individual fibers or propulsion of droplets on small groups of fibers [71].

Recent experimental data on wetting of individual polymer nanofibers [72] suggest that the difference of wetting behavior of nanofibers in comparison to flat surfaces can be attributed not only to size effects, but also to the different chemical properties of the nanofiber surface, induced by the fast electrospinning process.

Mattia et al. [73] investigated theoretically stationary profiles of drops and menisci on outer and inner surfaces of nanofibers and nanotubes as well as the stability of these profiles. The authors have introduced an effective disjoining/conjoining pressure, which includes, besides the classical disjoining/conjoining pressure isotherm, the radius of nanofiber/nanotube and surface tension. The stability criteria for the drops and menisci have been formulated in terms of the effective disjoining/conjoining pressure. It has been shown that the equilibrium contact angle is a function of the nanofiber/nanotube radius (cf. with the earlier results for the nanofiber [65]). The main mechanism of this dependence is the dependence of equilibrium uniform film (or adsorbed film) thickness on the radius.

The recent experimental works and molecular dynamic simulations on wetting of nanotubes are reviewed in [74]. The flow of liquids through the nanotubes is governed by the nanotube diameter, the surface chemistry and roughness. The unexpectedly high flow rates of liquids through carbon nanotube membranes has been attributed to a plug-form velocity profile with a jump near the liquid-solid interface. Interestingly, this characteristic velocity profile has been predicted not only for hydrophobic, but also for hydrophilic walls.

The water flow rate measurement through a nanoporous block copolymer membrane [75] brought opposite results: the measured flow rate corresponded to nanopores with diameter of 13.7 nm (under an assumption of Poiseuille flow), whereas the pore diameter independently measured by two different methods was 16.8 nm. The authors could not find any self-consistent explanation of the reduced flow rate. It should be noted that the chemical properties of the carbon nanotube membranes and block copolymer membranes are very different, which could account for qualitatively different wall-liquid forces at the inner side of the nanotube or nanopore.

In many applications the fibrous layers are comprised of flexible fibers. It has been shown that droplets wetting flexible nanofibers with a diameter below 500 nm may induce capillary buckling of the nanofibers [76]. However, the flexibility affects the wetting behavior of fibers even on a much larger scale. The combined effects of elasticity and capillarity on wetting of two parallel fibers with the diameter of hundreds of micrometers have been studied in [77,78]. Duprat et al. [77] investigated experimentally and theoretically the influence of fiber elasticity, the geometric parameters of the fibers and the droplet volume on the final wetting state. If the droplet volume is below a certain critical value, the droplet spreads in a column along the fibers which are deformed and coalesce. In a certain intermediate range of droplet volumes the column coexists with a compact barrel at an edge. For even larger droplet volume, the droplet spreading does not take place, and the droplet stays in a compact form of a barrel crossed by the fibers. Duprat

et al. [78] studied the diffusion-controlled evaporation of droplets on two parallel rigid and elastic fibers. Generally, the droplets in the column wetting state evaporate much faster than the droplets in the barrel wetting state, due to a higher area of the liquid-gas interface. It has been found for the rigid fibers that in the barrel (droplet) wetting state the evaporation rate is independent from the distance between the fibers, whereas for the column wetting state the evaporation rate increases with decreasing of the ratio between the distance between the fibers and the fiber radius. If the fibers are elastic, the wetting state and evaporation rate are influenced by the deformation of fibers. Interestingly, even if the initial wetting state is the barrel state, evaporation can lead to the transition the spread column state. This happens due to reduction of the droplet volume below the critical volume defined in [77]. This effect may lead to faster evaporation of liquid from fibrous media made of flexible material in comparison with the fibrous media made of rigid material.

3. Heat transport and phase change

Wetting of substrates with textured or porous coatings plays a prominent role in two-phase systems for cooling applications, including pool and flow boiling [79,80], jet and spray cooling [81–86], or cooling with liquid films [87]. In the following we mostly concentrate on heat transfer during impact of sprays and drops.

Spray cooling is a very effective means of heat removal from hot surfaces. Spray cooling is applied in the field of metal production, for the cooling of electronic modules and cryogen cooling of human tissues in medicine. Sprays provide a high contact surface between the heated surface and the cooler and may ensure a nearly constant temperature over a cooled area. The spray impact upon the surface creates a film upon it. This liquid film can be continuous or can contain holes which appear as a result of the film rupture. At low liquid flow rates and high heating rate the liquid is distributed on the surface in the form of separate sessile droplets and puddles. Further forms of liquid topology can be observed on the heated surface, depending on the spray characteristics, substrate topography, substrate wettability and temperature [81,82]. At high heating rates and, consequently, high surface temperatures, boiling occurs within the film created by spray. At surface temperatures significantly higher than the saturation temperature, the droplets do not reach the surface due to formation of a thin vapor layer over the surface. This phenomenon known as Leidenfrost effect leads to significant deterioration of heat transfer.

Heat convection and evaporation constitute the main mechanisms of heat transport during spray cooling. Convective heat transport is facilitated by large temperature difference between the substrate and spray liquid, by high outward velocity of liquid in the film and by high degree of mixing of liquid in the film, which takes place in the complex chaotic flow created by simultaneous impact and interaction of multiple droplets. Evaporation plays an important role in the cases where the gas phase is a pure vapor of the spray fluid and if the substrate temperature exceeds the saturation temperature. In the absence of boiling, the evaporation rate is limited by the thermal resistance between the hot substrate and the vapor. This resistance decreases with decreasing of the film thickness. In particular, the local evaporation rate is very high in the vicinity of the contact lines, where the film is extremely thin. Therefore, a high cumulative length of contact lines increases the evaporation rate and, therefore, the cooling efficiency [82].

Modification of hot substrate topography has been considered as a very promising method for heat transfer enhancement during spray cooling [81–86]. The typical substrate surface modifications included pin fins, straight fins, grooves and pyramids [82,84,86]. These modifications brought about significant heat transfer enhancement. Silk et al. [84] reported a 75% enhancement of Critical Heat Flux for 1 mm high straight fin topography with PF-5060 as working fluid at 41.4 kPa chamber pressure in pure vapor atmosphere. The authors don't provide an unambiguous explanation of enhancement mechanism. They suggest that the heat transfer in their system is dominated by flow boiling. The straight fins bring about increase in number of bubble nucleation sites and increase of drainage flow velocity. Sodtke and Stephan [82] have performed spray cooling experiments with deionized water in pure vapor atmosphere at superheat below 6 K, which precluded the onset of flow boiling in liquid film. The five-fold-factor enhancement of heat flux for micro pyramid structures at a flow rate of 16 kg/h has been attributed to topography-induced increase of cumulative length of contact line, leading to a drastic increase of evaporation rate. It has been suggested that the surface topography prevents the uncontrolled film dryout, which usually results in appearance of large dry areas which do not contribute to heat transport. Instead, the liquid is uniformly distributed over the substrate due to the action of capillary forces, so that only the peaks of micro pyramids stay dry, whereas the liquid flows in the valleys of the topography. Xie et al. [86] investigated the effect of enhanced surfaces on heat transfer enhancement during spray cooling of vertically oriented surface with R134a as test fluids. The highest (65%) heat transfer enhancement has been registered for multiscale-structured substrates consisting of 1 mm-scale topography with additional roughness elements on top of it.

It can be suggested that using microporous coating instead of topographical features such as fins, pillars, pyramids or grooves, would increase the capillary forces retaining more liquid distributed on the surface. Therefore, these coatings can potentially lead to intensification of evaporation. Several works have been devoted to investigation of spray cooling of substrates with microporous coatings. Kim et al. [83] have tested an effect of microporous coating consisting of aluminum particles with a binder, whereas the particle sizes varied for different experiment from 8-12 μm to 100-300 μm. The microporous coating was formed on a copper heater surface of an area 25 cm^2. The spray cooling experiments have been performed for the range of water flow rate between 1.25 and 3.0 ml/min. The spray was produced by an airbrush atomizer. The effect of microporous coating on heat transfer was negligible for the temperature difference between the substrate and ambient below 20 K. However, at higher temperature differences the heat transfer during spray cooling of a plain copper surface has been deteriorated due to the film dryout. The dryout was prevented on microporous coating, which lead to increase of dryout heat flux from 15 kW/m^2 (for the plain substrate) to 21 kW/m^2 (for the coated substrate). The authors have tested the effect of the coating thickness on heat transfer performance and found that 100 μm is the optimum thickness. Similar experiments have been performed by Kim et al. [85] for microporous coating based on diamond particles with the average particle size varying between 6 mm and 25 mm and coating thickness from 43 μm to 169 μm for different coatings. The heater area in this study was 4 cm^2. The main conclusions of the previous study have been confirmed.

Drop impact on hot substrates and concomitant heat transport phenomena are important processes involved in spray cooling. At the same time, the hydrodynamics, heat transfer and phase change during single drop impact are less complex than the transport processes in spray cooling and more easily accessible to many diagnostic techniques. Numerous experimental and theoretical/numerical works are devoted to drop impact visualization and at investigation of transport processes induced by drop impact. The drop impact process is governed by inertia, wetting, surface tension and viscosity. If the substrate is hot, evaporation may significantly affect both hydrodynamics and heat transport. The effect of evaporation manifests itself in boiling inside the drop in contact with the hot substrate, and, at higher substrate super heat, in Leidenfrost effect, in which the contact between the droplet and the substrate is precluded due to a thin vapor layer formed by evaporation at the early stages of the droplet impact. In Leidenfrost regime the heat transfer between the substrate and the liquid is extremely slow because of the insulating action of the vapor layer.

Since the transport processes during drop impact are governed by wetting, the modification of surface topography can be used to influence the heat transport. Bernardin et al. [88] have studied water drop

impact onto hot copper substrates with average roughness ranging from 97 nm to 2.96 μm to find that increasing surface roughness leads to (i) decreasing the droplet lifetime at temperatures corresponding to the nucleate boiling; (ii) violent breakup of the spreading liquid film at high temperatures corresponding to the film boiling and part of the transition boiling range. Fukuda et al. [89] investigated the water drop impact on hot stainless steel targets with average roughness ranging from Ra 0.04 (mirror) to Ra 10. The authors used high-speed video to estimate the contact time between the droplet and the hot surface. They found that the contact time increases on surface with the highest average roughness. It has been also found that the substrate cooling rate upon spray impingement increases with increasing average roughness.

Liu et al. [90] studied the heat transfer enhancement due to hydrophilic zeolite coating. The tests have been performed with water droplets gently deposited onto bare stainless steel substrates and steel substrates coated with zeolite microparticles. The substrates have been attached to massive heaters. It has been found that the minimal reachable temperature for the coated substrates with initial temperature of 200 °C was 105 °C, whereas for the bare steel surface the minimal temperature of 145 °C could be reached. The heat transfer enhancement has been attributed to the change of the substrate wettability. No experiments with drop impact cooling have been performed. It is not clear if the nanoporous zeolite structure had any influence on heat transfer.

The wetting and imbibition behavior of droplets impacting upon surfaces coated with nanofiber mats parallel to the surface plane ([11], see Section 2.1) makes these coatings attractive for heat transfer application. The first experiments devoted to studying the effect of nanofiber mats on heat transfer during drop impact on hot surfaces were performed with Polyacrylonitrile (PAN) electrospun nanofiber mats covering a 10 μm thick stainless steel foil [91]. The foil has been heated by electrical current with a constant power. The cooling experiments have been performed with droplets of a diameter around 2 mm gently deposited onto the surface or released from the height of 10 cm and 15 cm. The temperature evolution at the back side of the steel foil at the location of drop deposition/impact and at a distance of 1 cm from this location has been recorded with type K thermocouples. The cooling experiments have been repeated with bare steel foil for comparison. The first results have shown the striking heat transfer enhancement due to the nanofiber mat coating. First, the minimum temperature reached by drop impact cooling of the coated foil was around 8 K lower than that by the drop impact cooling of the uncoated foil. Second, the cooled area drastically increases in the presence of the nanofiber mat: a significant temperature decrease upon drop impact at the distance of 1 cm from the deposition/impact location was observed for the coated foil, whereas no cooling effect was registered at the same point for the uncoated foil. Third, the total droplet evaporation time significantly reduced on the foils coated with nanofiber mats, which indicates the increase of evaporation rate. The obtained results contradict the common intuition, since the nanofiber mat with porosity of about 90–95% might be expected to work as a thermal insulator. However, the full evaporation of impacting droplets is facilitated by the elimination of the drop splashing, bouncing and receding through the action of nanofiber mats [11]. The increase of the cooling area is caused by the imbibition of the liquid into the mat. Srikar et al. [91] have tested the thermal and structural properties of the nanofiber mats based on four different polymers. It has been found that the PAN and Poly(methylmethacrylate) (PMMA) nanofiber mats are stable in the temperature range at least up to 100 °C and can therefore be used for microelectronic applications, where the cooling demands are especially severe. Further investigations have shown that the PAN nanofiber mats can successfully survive applications at temperatures as high as 300 °C.

In [12] the heat transfer during drop impact onto heated steel foils coated with PAN nanofiber mats of different thicknesses and with PAN nanofiber mats containing carbon black nanoparticles (PAN + CB) has been studied simultaneously with the visualization of droplet spreading and imbibition. The temperature distribution inside this region was nearly uniform. A six-fold decrease of the droplet evaporation time on a foil coated with PAN + CB nanofiber mat in comparison with bare steel foil has been measured. The minimum temperature reached by drop impact onto the foil coated with the PAN + CB nanofiber mat is around 10 K lower in comparison with the bare steel foil in the range of initial foil temperatures from 60 °C to 100 °C. It has been suggested that the cooling efficiency of the nanofiber mats can be further increased by using nanofibers of material with high thermal conductivity.

Sinha-Ray et al. [92] coated copper substrates with 30 μm thick PAN nanofiber mats and electroplated them with four different metals: copper, silver, nickel, and gold. The aim of electroplating was to increase the thermal conductivity and diffusivity of fibers toward further heat transfer enhancement during droplet impact cooling. The copper-plated and silver-plated nanofibers are characterized by very rough surface with different kinds of nanotexture, whereas the surface of the gold-plated nanofibers was very smooth. The droplet evaporation time from metal-plated nanofiber mats was two orders of magnitude shorter than the droplet evaporation time from polymer mats reported in [12] at comparable drop impact conditions and initial substrate temperature. This difference can be explained by the superior thermal conductivity and diffusivity of the metal-plated fibers, the difference of the nanofiber surface properties (better wettability and higher surface area), but also by the difference of the heater design in both experiments (massive copper heater in the experiments with metal-plated nanofibers and thin stainless steel foil in the previous work). The average cooling heat flux due to droplet impact has been determined from the droplet evaporation time. The highest heat flux of 0.6 kW/cm^2 was reported for the copper-plated nanofiber mats, following by silver-plated nanofiber mats. Comparing the surface nanotextures of nanofibers plated by four different metals and the thermal diffusivities of these metals, the authors came to conclusion that the high heat flux is promoted by two simultaneous factors: high thermal diffusivity of the plated metal and rough surface of the metal-plated nanofibers.

Sinha-Ray and Yarin [93] have extended the studies of drop impact on copper-plate nanofiber mats to the train of droplets/jets issued with a controlled frequency. By varying the impact frequency of water droplets/jets in the range from 0.83 Hz to 10 Hz, with the average water mass flow varying in the range 4.8–8.7 mg/s, an optimal frequency of 4 Hz was shown to lead to a highest heat flux. At this frequency the liquid supply rate was equal to evaporation rate, and the time interval between successive drops/jets impact was short enough to prevent the appearance of dry spots. Sinha-Ray et al. [94] performed the experiment described in [93] in parabolic flight, thus under variable gravity acceleration (from microgravity to 1.8 g). It has been shown that the advantage of using the copper-plated nanofiber mats for drop cooling applications in comparison with bare copper surface was more pronounced for hypergravity conditions and less pronounced in microgravity conditions in comparison with terrestrial gravity.

It was known that the Leidenfrost temperature tends to increase on porous surfaces. The experiments of Avedisian and Koplik [95] have revealed that the Leidenfrost temperature for a stainless steel substrate coated with a 1.6 mm thick alumina layer of 10% porosity was around 100 K higher than that of a polished stainless steel surfaces; the Leidenfrost temperature of a 3.2 mm thick alumina substrate with a 25% porosity and particle size of 5–10 μm was nearly 200 K higher than that of a polished steel substrate. It has been suggested that some of the vapor generated by the droplet evaporation could be absorbed or percolated into the porous matrix, leading to decrease of the vapor layer thickness and its stability in comparison with that over an impermeable substrate. However, this explanation does not take into account the change of thermophysical properties of the porous coating or complete porous substrate compared with the properties of the steel substrate, as well as the change of thermal resistance between the heater and the substrate.

Later investigations on the effect of rough, porous and textured surfaces on Leidenfrost temperature lead to ambivalent results. Tran et al. [96] have found that the silicon substrates decorated with micropillars with diameter of 9 μm and heights varying between 2 μm and 8 μm lead to decrease of Leidenfrost temperature. Moreover, the parameter study revealed that the Leidenfrost temperature decreases with increasing micropillar height. Similar trends have been discovered for water drop evaporation on micropatterned metallic surfaces [97]. In this work two different types of substrate topography have been used: one consisting of blind microholes and another consisting of interconnected micropillars. The authors have determined the Leidenfrost temperature based on two kinds of observations: droplet evaporation time and apparent contact angle formed by the droplet. It was assumed that the Leidenfrost temperature corresponds to the maximal droplet evaporation time and to sharp increase of the apparent contact angle. The Leidenfrost temperature for the micropillars topography was around 140 °C and for microholes topography around 160 °C, whereas for the plain surface the Leidenfrost temperature of 245 °C has been determined. It should be noted that the experimentally determined Leidenfrost temperature corresponds to the so called pinned Leidenfrost state, where partial contact between the substrate and the drop still persists. At the substrate temperatures slightly below the Leidenfrost temperature intensive nucleate boiling has been observed on microstructured surfaces. It has been suggested that the microstructural features act as the bubbles nucleation sites promoting the formation of the liquid film as described in [98].

Kim et al. [99] studied the effects of sparsely arranged cylindrical micropillars, wettability, and nanoporosity on the Leidenfrost temperature. The wettability has been controlled by depositing thin gold layer (100 nm thick, contact angle for water droplets 83°) or thin silicon oxide layer (20 nm thick, contact angle 19°). The effect of nanoporosity has been tested by depositing a 600 nm thick nanoporous layer of silicon oxide nanoparticles (this procedure also lead to establishment of a contact angle of 0°). The Leidenfrost temperature has been determined from the maximal droplet evaporation time. It has been found that the nanoporosity has a decisive effect on the Leidenfrost phenomenon. The Leidenfrost temperature for the smooth gold surface without micropillars was measured to be 264 °C, for the smooth silicon oxide surface with micropillars 274 °C, for the nanoporous silicon oxide surface without micropillars 359 °C and for the nanoporous silicon oxide surface with micropillars 453 °C. Visual observations revealed violent splashes of small droplets around the evaporating droplet for the substrates with nanoporous coating at elevated temperatures. These splashes destabilize the vapor layer and suppress the Leidenfrost phenomenon. Kim et al. [99] believe that the key effect in suppressing the Leidenfrost phenomenon is the nucleation of bubbles during intermittent contact between the nanoporous substrate and the liquid.

Kwon et al. [100] studied the effect of surface microstructure consisting of micromillars array on Leidenfrost phenomenon. The authors have performed a parametric study to find the dependency of Leidenfrost temperature on the distance between the micropillars for water droplets. They found that the Leidenfrost temperature increases with increasing distance between the micropillars. The authors attribute this behavior to competing actions of capillary forces exerted by the micropillars and increasing hydrodynamic resistance for the escaping vapor due to the presence of micropillars. A further increase of the Leidenfrost temperature could be reached by combination of micropillars arrays with nanoparticles coating. In contrast to [99], Kwon et al. [100] attributed the influence of nanoparticles to the increase of capillary forces.

It has been discovered that nanofiber mats significantly suppress the Leidenfrost effect [101]. The droplet impact cooling experiments have been performed with a stainless steel foil covered by PAN + CB nanofiber mats heated by electrical current. Water and ethanol have been used as test fluids. The occurrence of the Leidenfrost regime could be determined from the visual observation and from the measurement of the steel foil temperature evolution. Since the Leidenfrost regime is characterized by a very low heat transfer rate between the substrate and the droplet, this regime manifested itself in very weak or no foil temperature reduction upon droplet impact. For the initial foil temperature of 180 °C and above, a transition to Leidefrost regime has been observed during impact of ethanol droplets upon a bare steel foil. For the initial foil temperatures of 220 °C and 300 °C, the drop impact did not lead to foil temperature reduction, which confirmed the suggestion that the droplet did not touch the hot surface. The situation was completely different for the foil coated with PAN + CB nanofiber mats. The impacted ethanol droplet was visibly attached to the substrate even at the temperature of 300 °C, and also penetrated into the mat (Fig. 6). The droplet evaporation led to significant foil temperature reduction: the minimum temperature of 190 °C has been reached for the initial foil temperature of 300 °C (Fig. 7). It is interesting to note that boiling regime was never observed upon drop impact onto a hot nanofiber mat unless the mat was damaged. The pores in the coating did not act as nucleation sites. The intensive evaporation took place from the partially wetted mat, exactly in the same way as previously described in [12].

Nair et al. [102] have found that the Leidenfrost effect is also suppressed by substrates decorated with carbon nanofiber, where the nanofibers are oriented normal to the substrate plane (different from the nanofibers arrangement used in [11,12,91,92,101]). The authors performed experiments with the 3 M Fluorinert Electronic Liquid FC-72. In their experiments the surface temperature varied between 60 °C and 450 °C, and the Weber number varied between 10 and 1000. The dynamic Leidenfrost temperature (the transition temperature between the contact evaporation/boiling regime and the Leidenfrost regime) has been determined by the analysis of high-speed image sequences as a function of Weber number for different substrates. It has been found that the dynamic Leidenfrost temperature increases with increasing the impact velocity, or the Weber

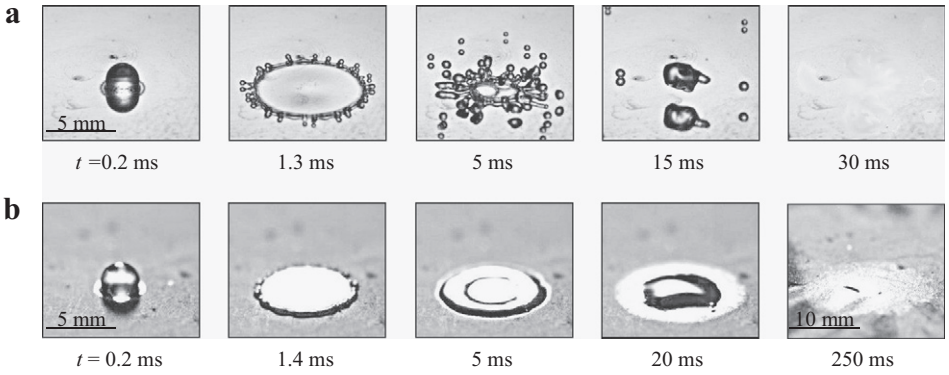

Fig. 6. Ethanol drop impact (a) on a bare steel foil and (b) on PAN + CB nanofiber mat with thickness 0.5 mm at an initial temperature of 300 °C (reproduced from [101]).

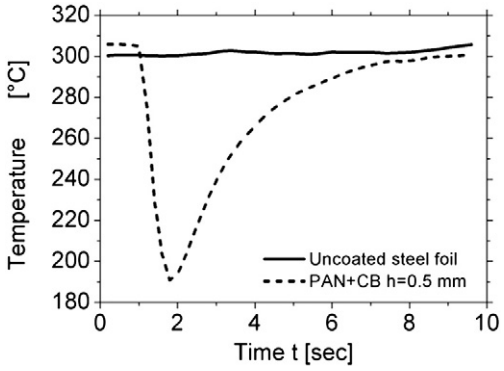

Fig. 7. Evolution of foil temperature under the ethanol drop impact point for initial foil temperature of 300 °C (reproduced from [101]).

number, both for the bare silicon substrates and for the substrates covered by carbon nanofibers. It has been also found that the dynamic Leidenfrost temperature is significantly higher for the substrates covered with nanofibers. For example, for We = 100, the Leidenfrost temperature for the bare silicon surface is 110 °C, and for the substrate decorated with carbon nanofibers of thickness ~7.5 μm the Leidenfrost temperature is as high as 350 °C. The authors stress that this trend is opposite to that detected for surfaces with micropillars [67]. For the microstructure surfaces the Leidenfrost temperature decreases in comparison with bare silicon substrate. Nair et al. [102] explain the difference by the cooling of nanofibers by the vapor. Due their small diameter, the nanofibers, in contrast to micropillars of comparable height, have enough time to be cooled by the vapor flow.

The effect of nanoporous coatings has been studied for the flow boiling in microchannels [79] and for pool boiling [80]. The effect of carbon nanotubes, which have been initially arranged normal to the copper surface, on flow boiling heat transfer was to enhance the heat transfer in the nucleate boiling region. This enhancement has been registered after the carbon nanotubes have been bent towards the copper surface by the water flow. Jun et al. [80] measured a drastic heat transfer enhancement by using copper-plated electrospun nanofibers in pool boiling experiments. The suggested enhancement mechanism was acceleration of the bubble growth rate, increase of the bubble detachment frequency and increase of density of nucleation sites due to the presence of nanofiber mat.

It can be seen from the above review that different mechanisms of the effect of (nano)porous coatings and substrate texture on heat transport have been suggested by different authors. These suggestions could be justified only implicitly, since the two-phase transport of fluids at the relevant scales is inaccessible for the conventional diagnostics. The rare experimental works devoted to transport processes in nanofiber mats provide only integrated data on temperature or moisture difference over nanofibers [103]. No attempt has been made so far to develop a numerical model describing heat transfer and phase change in processes where multiscale wetting phenomena are involved.

4. Particles transport and deposition

The transport and deposition of particles in porous media or thin porous layers is highly relevant for the ink-jet printing process applied to the 3D printing process [104], to functionalization of textile fabric as well as to printing of electronic circuits on paper and textile substrates [105].

Barani et al. [106] have loaded wool fabrics with silver nanoparticles to hydrophilize the fabric. The characterization of the treated wool fabrics on the micro- and nanoscale and characterization of wetting properties alteration has displayed a strong dependence on the method of nanoparticles deposition. Two out of three described loading methods (exhaustion and pad-dry-cure) have been based on immersing the fabric into a liquid containing silver nanoparticles and stabilizing agent with consequent heat treatment. In the pad-dry-cure method a squeezing step was introduced before the heat treatment. The difference in the final distribution of nanoparticle in the treated fabric has been apparently caused by the difference in nanoparticles transport during wetting, dewetting and drying phases of the fabric treatment.

Hamada et al. [107] characterized the rate of absorption of inks into nonwoven fabrics. They have also observed the microscale distribution of the inks in the fabric using a confocal laser scanning microscope. The distribution of ink pigments was different depending on the presence of latex coating over the fabric.

Dou and Derby [108] studied the formation of coffee stains during evaporation of nanoparticle suspension droplets on a porous substrate. They have found that the coffee stain effect is present for the porous substrate even in the cases where the suspension is optimized in such a way that this effect is absent on a solid impermeable substrate.

Venzmer [109] stresses the role of quats (cation surfactants) in the care products. One of the most important issues in formulation of care products is the deposition of caring substances on a surface, for example, hair or textile fiber. Deposition is normally facilitated by an attractive force between the caring agent and the surface. Since the most of the relevant surfaces carry an anionic surface charge, using cationic surfactants in combination with the caring substances evoke Coulomb attraction between the surface and the caring agent which facilitates deposition. In [109], the deposition of hair conditioning ingredients upon a damaged hair surface and deposition of quat vesicles on the cotton fabric fibers have been visualized using fluorescence microscopy. The final distribution of the deposited quat vesicles, which typically have a dimension of several micrometers, is governed, apart from the Coulomb forces, by the wetting of the fibrous layer and the penetration of the vesicles through the layer. The latter process depends on the size, shape and mechanical properties of the quat vesicles. By now, the mechanism of the wetting/penetration/deposition of quats has not been sufficiently studied. The typical efforts towards the improvement of the deposition process are focused on enhancement of the adherence of the caring substance to the surface [110].

Theoretical and numerical works on particles deposition during wetting are mostly limited to plain surfaces [111]. In contrast, the deposition of particles on textured or porous substrate did not gain much attention of scientific community involved in numerical work. Joshi and Sun [112] have used the lattice Boltzmann method to describe the spreading and evaporation of colloidal drops onto patterned or rough surfaces. The model developed by Joshi and Sun can be applied for prediction of transport phenomena during suspension drop evaporation for printable electronic fabrication. The simulations of suspension drop evaporation on a rough surface predicted a stick and slip behavior.

The author is unaware of attempts to develop a theoretical or numerical model for description of particles transport in porous/fibrous layers.

5. Concluding remarks and future research directions

The major mechanisms affecting the hydrodynamics of spreading and imbibition in porous layers are presently relatively good understood. However, the prediction of these processes with the goal of optimization of structure and properties for specific applications requires the knowledge of the effective properties of the porous media, accounting for the partial saturation of the material, the specific orientation of (nano)fibers and pores as well as the nanoscale effects. Further development of experimental and numerical tools for determination of these properties should become one of the priorities of future investigations. These studies can be supported by direct visualization of the time-dependent distribution of liquid in porous layers.

Presently, no dedicated model exists for description of dynamic contact line behavior on porous layers. In theoretical and numerical investigations of simultaneous spreading and imbibition the contact line models established for smooth solid substrates are used [25,27,42,50,56].

Surprisingly, only a few works are devoted to theoretical and numerical description of heat transport and phase change accompanying spreading and imbibition in porous materials. However, due to the increased interest in the role of porous coatings in heat transfer enhancement, a breakthrough in this topic can be expected in the next several years. Apart from the predictive tools, standardized experimental procedures should be developed, which will allow to qualify the influence of porous structure on heat transfer enhancement, with the thermal boundary conditions kept constant and not affecting the evaluation of the results.

In the field of particles transport and deposition on porous layers some efforts are expected towards the development of theoretical and numerical models which will reduce the number and range of trial and error experiments required to create new product formulation for industrial or domestic applications.

Acknowledgement

This review article has been prepared in the framework of the Marie Curie Initial Training Network “Complex Wetting Phenomena” (CoWet), Grant Agreement no. 607861.

References

[1] Deng X, Mammen L, Butt H-J, Vollmer D. Candle soot as a template for a transparent robust superamphiphobic coating. Science 2012;335:67–70. http://dx.doi.org/10.1126/science.1207115.
[2] Herminghaus S. Roughness-induced non-wetting. Europhys Lett 2000;52:165–70.
[3] Daniel RC, Berg JC. Spreading on and penetration into thin, permeable print media: Application to ink-jet printing. Adv Colloid Interf Sci 2006;123-126:439–69.
[4] De Gennes P. Wetting: Statics and dynamics. Rev Mod Phys 1985;57:827–63.
[5] Washburn EW. The dynamics of capillary flow. Phys Rev 1921;17:273–83.
[6] Marmur A. The radial capillarity. J Colloid Interface Sci 1988;124:301–8.
[7] Pezron I, Bourgain G, Quéré D. Imbibition of a fabric. J Colloid Interface Sci 1995;173:319–27.
[8] Bormashenko E, Starov V. Impact of surface forces on wetting of hierarchical surfaces and contact angle hysteresis. Colloid Polym Sci 2013;291:343–6.
[9] Bormashenko E, Bormashenko Y, Pogreb R, Stanevsky O, Whyman G. Droplet behavior on flat and textured surfaces: Co-occurrence of Deegan outward flow with Marangoni solute instability. J Colloid Interface Sci 2007;306:128–32.
[10] Papodopoulos P, Mammen L, Deng X, Vollmer D, Butt H-J. How superhydrophobicity breaks down. PNAS 2013;110:3254–8.
[11] Lembach AN, Tan H-B, Roisman IV, Gambaryan-Roisman T, Zhang Y, Tropea C, et al. Drop impact, spreading, splashing and penetration into electrospun nanofiber mats. Langmuir 2009;26(12):9516–23. http://dx.doi.org/10.1021/la100031d.
[12] Weickgenannt CM, Zhang Y, Lembach AN, Roisman IV, Gambaryan-Roisman T, Yarin AL, et al. Non-isothermal drop impact and evaporation on polymer nanofiber mats. Phys Rev E 2010;83(3):036305. http://dx.doi.org/10.1103/PhysRevE.00.006300.
[13] Bacri L, Brochard-Wyart F. Droplet suction on porous media. Eur Phys J E 2000;3:87–97.
[14] Bico J, Tordeax C, Quéré D. Rough wetting. Europhys Lett 2001;55:214–20.
[15] Bormashenko E. Wetting of real surfaces. Berlin/Boston: De Gruyer; 2013.
[16] De Gennes P-G, Brochard-Wyart F, Quéré D. Capillarity and wetting phenomena: Drops, bubbles, pearls, waves. New York: Springer; 2004.
[17] Courbin L, Bird JC, Reyssat M, Stone HA. Dynamics of wetting: from inertial spreading to viscous imbibition. J Phys Condens Matter 2009;21:464127.
[18] Quéré D. Inertial capillarity. Europhys Lett 1997;39:533–8.
[19] Marmur A. Penetration of a small drop into a capillary. J Colloid Interface Sci 1988;122:209–19.
[20] Zhmud BW, Tiberg F, Hallstensson K. Dynamics of capillary rise. J Colloid Interface Sci 2000;228:263–9.
[21] Ishino C, Reyssat M, Reyssat E, Okumura K, Quéré D. Wicking within forest of micropillars. Europhys Lett 2007;79:56005.
[22] Cassie ABD, Baxter S. Wettability of porous surfaces. Trans Faraday Soc 1944;40:0546–50.
[23] Wenzel RN. Resistance of solid surfaces to wetting by water. Ind Eng Chem 1936;28:988–94.
[24] Boreyko JB, Baker CH, Poley CR, Chen C-H. Wetting and dewetting transitions on hierarchical superhydrophobic surfaces. Langmuir 2011;27:7502–9.
[25] Hilpert M, Ben-David A. Infiltration of liquid droplets into porous media: Effects of dynamic contact angle and contact angle hysteresis. Int J Multiphase Flow 2009;35:205–18. http://dx.doi.org/10.1016/j.ijmultiphaseflow.2008.11.007.
[26] Leese H, Bhurtun V, Lee KP, Mattia D. Wetting behaviour of hydrophilic and hydrophobic nanostructured porous anodic alumina. Colloids Surf A Physicochem Eng Asp 2013;420:53–8.
[27] Davis SH, Hocking LM. Spreading and imbibition of viscous liquid on a porous base. II. Phys Fluids 2000;12(7):1646–55.
[28] Grzelakowski C, Ben Jazia D, Lebeau B, Vonna L, Dupuis D, Haidara H. On the influence of pore structure on the free-imbibition of sessile drops into nanoporous substrates. Langmuir 2009;25:5855–60. http://dx.doi.org/10.1021/la803465u.
[29] Lafuma A, Quéré D. Superhydrophobic states. Nat Mater 2003;2:457–60.
[30] Dash S, Garimella SV. Droplet evaporation dynamics on a superhydrophobic surface with negligible hysteresis. Langmuir 2013;29:10785–95.
[31] Herminghaus S, Brinkmann M, Seemann R. Wetting and dewetting of complex surface geometries. Annu Rev Mater Res 2008;38:101–21.
[32] Sahu RP, Sinha-Ray S, Yarin AL, Pourdeyhimi B. Drop impacts on electrospun nanofiber membranes. Soft Matter 2012;8:3957–70.
[33] Moulinet S, Bartolo D. Life and death of a fakir droplet: Impalement transitions on superhydrophobic surfaces. Eur Phys J E 2007;24:251–60.
[34] Reyssat M, Yeomans JM, Quéré D. Impalement of fakir drops. Europhys Lett 2008;81:26006.
[35] Sbragaglia M, Peters AM, Pirat C, Borkent BM, Lammertink RGH, Wessling M, et al. Spontaneous breakdown of superhydrophobicity. Phys Rev Lett 2007;99:156001.
[36] Pirat C, Sbragaglia M, Peters AM, Borkent BM, Lammertink RGH, Wessling M, et al. Multiple time scale dynamics in the breakdown of hydrophobicity. Europhys Lett 2008;81:66002.
[37] Emami B, Tafreshi HV, Gad-el-Hak M, Tepper GC. Effect of fiber orientation on shape and stability of air-water interface on submerged superhydrophobic electrospun thin coatings. J Appl Phys 2012;111(6):064325. http://dx.doi.org/10.1063/1.3697895.
[38] Starov VM, Kosvintsev SR, Sobolev VD, Velarde MD, Zhdanov SA. Spreading of liquid drops over saturated porous layers. J Colloid Interface Sci 2002;246:372–9.
[39] Starov VM, Kosvintsev SR, Sobolev VD, Velarde MG, Zhdanov SA. Spreading of liquid drops over dry porous layers: Complete wetting case. J Colloid Interface Sci 2002;252:397–408.
[40] Starov VM, Zhdanov SA, Velarde MG. Spreading of liquid drops over thick porous layers: complete wetting case. Langmuir 2002;18:9744–50.
[41] Starov VM, Zhdanov SA, Kosvintsev SR, Sobolev VD, Velarde MG. Spreading of liquid drops over porous substrates. Adv Colloid Interf Sci 2003;104:123–58. http://dx.doi.org/10.1016/S0001-8686(03)00039-3.
[42] Clarke A, Blake TD, Carruthers K, Woodward A. Spreading and imbibition of liquid droplets on porous surfaces. Langmuir 2002;18:2980–4.
[43] Lembach AN, Roisman IV, Tropea C. Drop impact on porous media. Proceeding of ILASS – Europe 2011, 24th European Conference on Liquid Atomization and Spray Systems, Estoril, Portugal; September 2011.
[44] Singh SK, Khandekar S, Pratap D, Anantha Ramakrishna S. Wetting dynamics and evaporation of sessile droplets on nano-porous alumina surfaces. Colloids Surf A Physicochem Eng Asp 2013;432:71–81.
[45] Li G, Zhao Y, Lv M, Shi Y, Cao D. Super hydrophilic poly(ethylene terephthalate) (PET)/poly(vinyl alcohol)(PVA) composite fibrous mats with improved mechanical properties prepared via electrospinning process. Colloids Surf A Physicochem Eng Aspects 2013;436:417–24.
[46] Wang L, Zhao Y, Wang J, Hong X, Zhai J, Jiang L, et al. Ultra-fast spreading on superhydrophilic fibrous mesh with nanochannels. Appl Surf Sci 2009;255:4944–9.
[47] Luikov AV. Heat and mass transfer in capillary-porous bodies. Oxford, U.K: Pergamon Press; 1966.
[48] Chong WY, Lim KS, Kim WH, Harun SW, Mahamd Adikan FR, Ahmad H. Spreading profile of evaporating liquid drops in thin porous layer. Phys Rev E 2012;85:016314.
[49] Huh C, Scriven LE. Hydrodynamic model of a steady movement of a solid/liquid/fluid contact line. J Colloid Interface Sci 1971;35:85–101.
[50] Zadražil A, Stepanek F, Matar OK. Droplet spreading, imbibition and solidification on porous media. J Fluid Mech 2006;562:1–33. http://dx.doi.org/10.1017/S0022112006000875.
[51] Davis SH, Hocking LM. Spreading and imbibition of viscous liquid on a porous base. Phys Fluids 1999;11(1):48–57.
[52] Oron A, Davis SH, Bankoff SG. Long - scale evolution of thin liquid films. Rev Mod Phys 1997;69:941–80.
[53] Zhdanov SA, Starov VM, Sobolev VD, Velarde MG. Spreading of aqueous SDS solutions over nitrocellulose membranes. J Colloid Interface Sci 2003;264:481–9.
[54] Hoffman RL. A study of the advancing interface. J Colloid Interface Sci 1975;50:228–41.
[55] Frank X, Perré P. Droplet spreading on a porous surface: A lattice Boltzmann study. Phys Fluids 2012;24:042101.
[56] Alleborn N, Raszillier H. Spreading and sorption of droplets on layered porous substrates. J Colloid Interface Sci 2004;280:449–64.
[57] Mao N, Russell SJ. Capillary pressure and liquid wicking in three-dimensional nonwoven materials. J Appl Phys 2008;104:034911. http://dx.doi.org/10.1063/1.2965188.
[58] Fatt I. The network model of porous media III. Dynamic properties of networks with tube radius distribution. Trans AIME 1956;207:164–81.
[59] Philip JR. Flow in porous media. Annu Rev Fluid Mech 1970;2:177–204.

[60] Markicevic B, Navaz HK. Primary and secondary infiltration of wetting liquid sessile droplet into porous medium. Transp Porous Media 2010;85:953–74. http://dx.doi.org/10.1007/s11242-010-9603-y.
[61] Delbos A, Lorenceau E, Pitois O. Forced impregnation of a capillary tube with drop impact. J Colloid Interface Sci 2010;341:171–7.
[62] Ding H, Theofanous TG. The inertial regime of drop impact on an anisotropic porous substrate. J Fluid Mech 2012;691:546–67. http://dx.doi.org/10.1017/jfm.2011.491.
[63] Yue P, Renardy Y. Spontaneous penetration of a non-wetting drop into an exposed pore. Phys Fluids 2013;25:052104. http://dx.doi.org/10.1063/1.4804957.
[64] Roisman IV, Weickgennant CM, Lembach AN, Tropea C. Drop impact close to a pore: experimental and numerical investigations. Proceeding of ILASS – Europe 2010, 23th European Conference on Liquid Atomization and Spray Systems, Brno, Czech Republic; September 2010.
[65] Neimark AV. Thermodynamic equilibrium and stability of liquid films and droplets on fibers. J Adhes Sci Technol 1999;13:1137–54.
[66] Barber AH, Cohen SR, Wagner HD. External and internal wetting of carbon nanotubes with organic liquids. Phys Rev B 2005;71:115443.
[67] Yum K, Yu M-F. Measurement of wetting properties of individual boron nitride nanotubes with the Wilhelmy method using a nanotube-based force sensor. Nano Lett 2005;6:329–33.
[68] Rossi MP, Ye H, Gogotsi Y, Babu S, Ndungu P, Bradley J-C. Environmental scanning electron microscopy study of water in carbon nanopipes. Nano Lett 2004;4:989–93.
[69] Yarin AL, Liu W, Reneker DH. Motion of droplets along thin fibers with temperature gradient. J Appl Phys 2002;91:4751–9.
[70] Yarin AL, Chase GG, Liu W, Doiphode SV, Reneker DH. Liquid drop growth on a fiber. AIChE J 2006;52:1–11.
[71] Keis K, Kornev KG, Kamath YK, Neimark AV. Towards fiber-based micro- and nanofluidics. In: Guceri S, Gogotsi YG, Kuznetsov V, editors. Nanoengineered nanofibrous materials. The Netherlands: Kluwer Academic Publishers; 2004. p. 175–82.
[72] Stachewicz U, Barber AH. Enhanced wetting behavior at electrospun polyamide nanofiber surfaces. Langmuir 2011;27:3024–9.
[73] Mattia D, Starov V, Semenov S. Thickness, stability and contact angle of liquid films on and inside nanofibres, nanotubes and nanochannels. J Colloid Interface Sci 2012;384:149–56.
[74] Bekou S, Mattia D. Wetting of nanotubes. Curr Opin Colloid Interface Sci 2011;16:259–65.
[75] Phillip WA, Rzayev J, Hillmyer MA, Cussler EL. Gas and water liquid transport through nanoporous block copolymer membranes. J Membr Sci 2006;286:144–52.
[76] Wu X-F, Bedarkar A, Akhatov IS. Hydroelastic analysis of an axially loaded compliant fiber wetted with a droplet. J Appl Phys 2010;108:083518.
[77] Duprat C, Protière S, Beebe AY, Stone HA. Wetting of flexible fiber arrays. Nature 2012;482:510–3.
[78] Duprat C, Bick AD, Warren PB, Stone HA. Evaporation of drops on two parallel fibers: Influence of the liquid morphology and fiber elasticity. Langmuir 2013;29:7857–63.
[79] Khanikar V, Mudawar I, Fisher T. Effects of carbon nanotube coating on flow boiling in a micro-channel. Int J Heat Mass Transf 2009;52:3805–17.
[80] Jun S, Sinha-Ray S, Yarin AL. Pool boiling on nano-textured surfaces. Int J Heat Mass Transf 2013;62:99–111.
[81] Kim J. Spray cooling heat transfer: The state of the art. Int J Heat Mass Transf 2007;28:753–67.
[82] Sodtke C, Stephan P. Spray cooling on micro structured surfaces. Int J Heat Mass Transf 2007;50:4089–97.
[83] Kim JH, You SM, Choi US. Evaporative spray cooling of plain and microporous coated surfaces. Int J Heat Mass Transf 2004;47:3307–15.
[84] Silk EA, Kim J, Kiger K. Spray cooling of enhanced surfaces: Impact of structured surface geometry and spray axis inclination. Int J Heat Mass Transf 2006;49:4910–20.
[85] Kim Y-H, Choi C, Lee K-J, Han D. Experimental study of spray cooling performance on micro-porous coated surfaces. Heat Mass Transf 2009;45:1285–92.
[86] Xie JL, Tan YB, Duan F, Ranjith K, Wong TN, Toh KC, et al. Study of heat transfer enhancement for structured surfaces in spray cooling. Appl Therm Eng 2013;59:464–72.
[87] Gambaryan-Roisman T, Stephan P. Analysis of falling film evaporation on grooved surfaces. J Enhanced Heat Transf 2003;10:445–57.
[88] Bernardin JD, Stebbins CJ, Mudawar I. Effects of surface roughness on water droplet impact history and heat transfer regimes. Int J Heat Mass Transf 1997;40:73–88.
[89] Fukuda S, Kohno M, Tagashira K, Ishihara N, Sumitomo H, Takata Y. Behavior of small droplet impinging on a hot surface. Heat Transfer Eng 2014;35:204–11.
[90] Liu J, Aguilar G, Munoz R, Yan Y. Hydrophilic zeolite coatings for improved heat transfer: A quantitative analysis. AIChE 2008;54:779–90.
[91] Srikar R, Gambaryan-Roisman T, Steffes C, Stephan P, Tropea C, Yarin A. Nanofiber coating of surfaces for intensification of spray or drop impact cooling. Int J Heat Mass Transf 2009;52:5814–26. http://dx.doi.org/10.1016/j.ijheatmasstransfer.2009.07.021.
[92] Sinha-Ray S, Zhang Y, Yarin AL. Thorny devil nanotextured fibers: the way to cooling rates on the order of 1 kW/cm^2. Langmuir 2011;27(1):215–26. http://dx.doi.org/10.1021/la104024t.
[93] Sinha-Ray S, Yarin AL. Drop impact cooling enhancement on nano-textured surfaces. Part I: Theory and results of the ground (1 g) experiments. Int J Heat Mass Transf 2014;70:1095–106.
[94] Sinha-Ray S, Sinha-Ray S, Yarin AL, Weickgenannt CM, Emmert J, Tropea C. Drop impact cooling enhancement on nano-textured surfaces. Part II: Results of the parabolic flight experiments [zero gravity (0 g) and supergryvity (1.8 g)]. Int J Heat Mass Transf 2014;70:1107–14.
[95] Avedisian CT, Koplik J. Leidenrost boiling of methanol droplets on hot porous/ceramic surfaces. Int J Heat Mass Transf 1987;30:379–93.
[96] Tran T, Staat HJJ, Susarrey-Arce A, Foertsch TC, van Houselt A, Gardeniers JGE, et al. Droplet impact on superheated micro-structured surfaces. Soft Matter 2013;9:3272–82.
[97] Del Cerro DA, Martin AG, Römer GRBE, Pathiraj B, Lohse D, in't Veld AJH. Leidenfrost point reduction on micropatterned metallic surfaces. Langmuir 2012;28:15106–10.
[98] Bernardin J, Mudawar I. A cavity activation and bubble growth model of the Leidenfrost point. J Heat Transf 2002;124:864–74.
[99] Kim H, Truong B, Buongiorno J, Hu L-W. On the effect of surface roughness height, wettability and nanoporosity on Leidenfrost phenomena. Appl Phys Lett 2011;98:083121.
[100] Kwon H-M, Bird JC, Varanasi KK. Increasing Leidenfrost point using micro-nano hierarchical surface structures. Appl Phys Lett 2013;103:201601.
[101] Weickgenannt CM, Zhang Y, Sinha-Ray S, Roisman IV, Gambaryan-Roisman T, Tropea C, et al. The inverse-Leidenfrost phenomenon on nanofiber mats on hot surfaces. Phys Rev E 2011;84:036310. http://dx.doi.org/10.1103/PhysRevE.84.036310.
[102] Nair H, Staat HJJ, Tran T, van Houselt A, Prosperetti A, Lohse D, et al. Leidenfrost temperature increase for impacting droplets on caron-nanofiber surfaces. Soft Matter 2013. http://dx.doi.org/10.1039/C3SM52326H.
[103] Borhani S, Etemad SG, Hosseini Ravandi SA. Dynamic heat and moisture transfer in bulky PAN nanofiber mats. Heat Mass Transf 2011;47:807–11.
[104] Butscher A, Bohner M, Hofmann S, Gauckler L, Müller R. Structural and material approaches to bone tissue engineering in powder-based three-dimensional printing. Acta Biomater 2011;7:907–20.
[105] Irurzun UB, Dutschk V, Calvimontes A, Akkerman R. Generation of micro-sized conductive lines on glass fibre fabrics by inkjet printing. AUTEX Res J 2012;12:55–60.
[106] Barani H, Montazer M, Calvimontes A, Dutschk V. Surface roughness and wettability of wool fabrics loaded with silver nanoparticles: Influence of synthesis and application methods. Text Res J 2013;83:1310–8.
[107] Hamada H, Bousfield DW, Luu WT. Absorption mechanism of aqueous and solvent inks into synthetic nonwoven fabrics. J Imaging Sci Technol 2009;53:050201.
[108] Dou R, Derby B. Formation of coffee stains on porous surfaces. Langmuir 2012;28:5331–8.
[109] Venzmer J. Hairs, cars, textile: In quats we care. SOFW J 2010;136(3):62–71.
[110] Herrwerth S, Ulrich-Brehm I, Kortemeier U, Winter P, Ferenz M, Grüning B. Silicone Quarternium-22: New Silicone Technology for premium hair conditioning with additional benefits. SOFW J 2009;135(6):1–7.
[111] Craster RV, Matar OK, Sefiane K. Pinning, retraction, and terracing of evaporating droplets containing nanoparticles. Langmuir 2009;25:3601–9.
[112] Joschi AS, Sun Y. Numerical simulation of colloidal drop deposition dynamics on patterned substrates for printable electronic fabrication. J Disp Technol 2010;6:579–85.